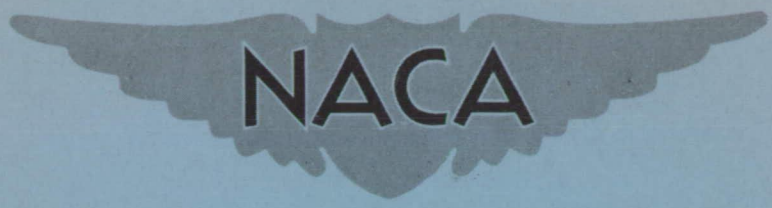RML58D18a

Copy 200
RM L58D18a

NACA

RESEARCH MEMORANDUM

TELEMETER TRANSMISSION AT

219.5 MEGACYCLES FROM TWO ROCKET-POWERED MODELS

AT MACH NUMBERS UP TO 15.7

By George B. Graves, Jr., and J. Thomas Markley

Langley Aeronautical Laboratory
Langley Field, Va.

NATIONAL ADVISORY COMMITTEE
FOR AERONAUTICS

WASHINGTON

July 28, 1958

NATIONAL ADVISORY COMMITTEE FOR AERONAUTICS

RESEARCH MEMORANDUM

TELEMETER TRANSMISSION AT

219.5 MEGACYCLES FROM TWO ROCKET-POWERED MODELS

AT MACH NUMBERS UP TO 15.7[*]

By George B. Graves, Jr., and J. Thomas Markley

SUMMARY

Successful telemeter transmission at hypersonic speeds was obtained from two five-stage rocket-powered models which used radio telemeters operating at a frequency of 219.5 megacycles. One model reached a Mach number of 15.5 at an altitude of 98,000 feet and the other model reached a Mach number of 15.7 at 70,500 feet altitude before the telemeter signal was lost. At Mach numbers above 5.0 comparison was made of the received signal strength with the predicted signal strength based on free-space theory for the expected flight paths. This comparison indicated that significant attenuation occurred during the period of Mach number increase. Attenuation may have resulted from thermal ionization in the high temperature gases surrounding the model or conditions in the exhaust gases during rocket burning; however, the results may have been caused by other factors, such as changes in model attitude which placed the receiving antenna in a null in the radiation pattern or losses in the antenna dielectric material at increased temperature.

INTRODUCTION

For some time it has been evident that radio transmission from a missile traveling at hypersonic speeds may be impaired because of ionization and free electrons in the high-temperature gases surrounding the missile. Since radio telemetry has become almost essential for obtaining data during the development and testing of missiles, and tactical use of missiles may require radio techniques for guidance and fusing, this could have serious effect on the development and use of long-range ballistic missiles and other hypersonic weapons. Theoretical analysis of the transmission and propagation problem is extremely difficult and requires information which is not available, such as

---

[*]Title, Unclassified.

details of the physical state of the gases surrounding the missile (including the degree of dissociation, ionization, and recombination rates) and knowledge of the interaction of these gases with the electromagnetic field of the transmitting antenna. Because of the small amount of experimental information available, a study has been made of the telemeter transmission from two free-flight rocket-powered research models which reached hypersonic speeds.

These rocket models were flown at the Langley Pilotless Aircraft Research Station at Wallops Island, Va., as part of a basic research program being conducted by the Langley Laboratory on the problems associated with hypersonic flight. While radio telemetry has been successfully used in obtaining data from a number of free-flight research models which have been flown as part of this program, the signal-strength measurements which are necessary in a study of the radio transmission problem were not made during previous model flights.

In order to indicate the attenuation resulting at increased velocities, the variation in signal strength received from telemeters operating at 219.5 megacycles is compared with calculated values based on free-space conditions. This comparison is made at flight conditions above a Mach number of 5.0 until the time of loss of telemeter signal, which occurred in one case at a Mach number of 15.5 at an altitude of 98,000 feet, and in the other case at a Mach number of 15.7 at an altitude of 70,500 feet. It is necessary to emphasize that the attenuation values are of a qualitative nature because of limitations in accurately determining the free-space antenna radiation patterns and difficulty in determining the attitude angles of the model which are needed to locate the position of the receiving site in these patterns.

An analysis is made of the heating conditions which apparently caused structural failure and loss of telemeter signal from one model. Analysis of the heating conditions for the other model indicates that the loss of telemeter signal in this case may also have been a result of structural failure caused by heating, although the heating conditions did not appear to be so severe as in the case of the first model. Some of the flight conditions are shown to correspond with points on the trajectory of a reentry missile with $\frac{W}{C_D A}$ of 100 lb/sq ft, a reentry

velocity of 20,000 feet per second, and a reentry angle of -21.8°. The electron concentration calculated at the stagnation point for the highest velocity flight conditions at which a telemeter signal was received approached maximum electron concentration expected during reentry of such a missile.

SYMBOLS

A   frontal area of body

C_D drag coefficient

d   distance, ft

G_R receiving antenna gain

G_T transmitting antenna gain

M   Mach number

Ne^- free electron concentration

P_T transmitted power, watts

P_R received power, watts

W   weight, lb

α angle relative to horizontal, deg

γ ratio of specific heat at constant pressure to specific heat
             at constant volume

λ wavelength, ft

Subscript:

w   air at temperature of wall

MODELS AND INSTRUMENTATION

Models

Each of the two models was propelled by a five-stage rocket system:
the first stage consisted of an M6 JATO (Honest John) rocket motor; the
second and third stages, M5 JATO (Nike) rocket motors; the fourth stage,
a JATO, 1.52-KS-33, 550, XM19 (Recruit) rocket motor; and the fifth
stage, a JATO, 1.3-KS-4800, T55 rocket motor. A photograph of one com-
plete assembly mounted on the launcher just prior to firing is shown in

figure 1. Figure 2 presents a sketch of the first four stages together with a table which gives the weights of the various components.

A photograph of model A is presented in figure 3 and a sketch is shown in figure 4. Model B is shown in the photograph of figure 5 and the sketch in figure 6.

Instrumentation

Both models were instrumented with standard NACA radio telemetry which uses a transmitter operating at 219.5 megacycles with a nominal radio-frequency power output of 1.5 watts. Measurements taken by five accelerometers and six thermocouples were transmitted from model A for the purpose of obtaining heating data. A detailed description of this model and the results of the heating investigation are given in reference 1. In model B, the instrumentation weight was held to a minimum in order to obtain maximum velocity, and longitudinal acceleration was the only measurement transmitted from the model.

Details of the antenna construction for model A are shown in figure 7. The measured radiation patterns for model A alone and for model A assembled with the fourth-stage Recruit rocket are presented in figure 8. Details of the antenna construction for model B are shown in figure 9, and the antenna radiation patterns for model B are presented in figure 10. In figure 10 the pattern for model B alone was measured; however, the pattern for model B assembled with the fourth stage was assumed to be identical with the pattern of model A assembled with its fourth stage.

The antenna radiation patterns which are presented in figures 8 and 10 are based on measurements made with the model and the receiving antenna separated by a distance of 300 feet and with both antennas located four wavelengths above the ground. Since several buildings are located within 1,000 feet of the antenna test area, there is a possibility that these patterns are in error, particularly at the lower signal levels where the reflected energy from the major lobes may represent an appreciable part of the power being measured. The results obtained from measurements made with antennas whose radiation patterns are well known indicate that portions of the antenna patterns which are within 6 decibels of the maximum value are accurate within ±2 decibels.

During the flight tests, the telemeter transmission was recorded by an NACA receiving station located at the launching site. The following receiving components were used:

(1) Antenna - Twenty-turn helix operated in its axial mode; circularly polarized; theoretical gain of 18 decibels over an isotropic radiator; 26° beam width at 3-decibel attenuation points

(2) Preamplifier - Applied Science Corporation of Princeton type APA-2 preamplifier; gain of 15 decibels; 4.5-decibel measured noise figure of preamplifier-telemeter receiver combination

(3) Receiver - NACA modified APR-4 receiver with intermediate-frequency band width of 2 megacycles and provisions for signal strength recording

A photograph of the receiving antenna used is shown in figure 11. The antenna was continuously directed at the model by an operator who was supplied information from the NACA modified SCR-584 tracking radar up until the time of fourth-stage firing. After this time the antenna was directed in accordance with a previously calculated trajectory. Comparison of the trajectory used for directing the antenna with the trajectory obtained after final data workup indicated that the antenna was positioned so that its gain was within 2 decibels of maximum during the tests.

DETERMINATION OF RECEIVED SIGNAL STRENGTH

The signal level at the intermediate frequency amplifier in the receiver was rectified, filtered, and recorded; and calibrations were made immediately following each flight to obtain the signal power received at the antenna terminals. The accuracy of this measurement was determined by the accuracy of the signal source and attenuators used for the calibrations and the stability of the receiving equipment. Comparison of a number of calibrations and laboratory tests of the commercial radio-frequency signal generator used indicated that the absolute accuracy was within ±3 decibels at power levels from 1×10^{-12} watts to 1×10^{-9} watts. Laboratory tests of the attenuators used and the agreement of repeated calibrations indicated that changes in power level were measured within ±0.5 decibel over the short interval of time required for the model flight and calibration of the receiving equipment. It was not possible to obtain reliable measurement of the received signal power at levels below 1.0×10^{-13} watts because of the thermal noise and interference present at this power level.

The power expected at the receiving antenna was calculated by using free-space transmission theory as presented in reference 2 and the relation

$$P_R = P_T\left(\frac{\lambda}{4\pi d}\right)^2 G_R G_T$$

The transmitted power was measured prior to firing each model and the gain of the transmitting antenna was obtained from the radiation patterns presented as figures 8 and 10 by determining the angle of the receiving site off the longitudinal axis of the model at each time point. It was assumed that the longitudinal axis of the model was alined with the tangent to the model flight path at all times. The angle between the tangent to the flight path and a line to the receiving site was then used to determine the position of the receiving site in the radiation pattern of the model. The angle of the receiving site off the longitudinal axis for models A and B is presented in figures 12 and 13, respectively.

The measured receiving antenna gain of 14 decibels over a half-wavelength dipole was used rather than the theoretical gain. The distance to the model was obtained from radar flight-path data discussed in the following section.

TESTS

Model A

Model A was launched at an angle of 73° and followed the flight path shown in figure 14. Up to the firing of the fourth stage, the information in figure 14 was obtained directly from the NACA modified SCR-584 radar. After this time radar tracking was intermittent, and it was necessary to base the data on velocities obtained by integrating the time history of the longitudinal accelerometer installed in the model.

The third stage of model A ignited at an angle of 5.8° with the horizontal at an altitude of 96,000 feet and Mach number of 1.0. The telemeter signal was continuous until failure occurred near the end of thrust of the last stage at 92.36 seconds after take-off. At this time, the model was at an altitude of 98,000 feet and the Mach number was 15.5.

Model B

Model B was launched at an angle of 74° from the horizontal and followed the flight path shown in figure 15. This flight-path information was obtained in the same manner as that for model A.

The third stage of model B was ignited at an angle of -17° with the horizontal at an altitude of 88,000 feet and a Mach number of 1.0. The telemeter signal was continuous until failure occurred near the end of thrust of the last stage at 94.71 seconds after take-off. At this time the model was at an altitude of 70,500 feet and the Mach number was 15.7.

Test Conditions

Atmospheric temperature and density information was obtained at the time of each model flight by the use of radiosonde equipment. These data were essentially the same for both model flights at the altitudes of interest. Figure 16 shows the atmospheric temperature and density at altitudes above 55,000 feet for both model flights.

Time histories showing the velocity and density for models A and B are shown in figures 17 and 18.

Model Temperatures

Maximum measured inside skin temperatures on model A reached 2,930° R at the time at which the telemeter signal was lost. Figure 19 presents time histories of the inside skin temperatures measured at two locations on the nose of model A. As discussed in reference 1, temperature differences through the skin of several hundred degrees were calculated near the end of the test. The resulting maximum temperatures indicate that the melting temperature of Inconel, 2,960° R, was reached on the surface and was closely approached on the inside of the skin at the time the telemeter signal was lost.

No temperatures were measured on model B; however, the wall temperatures were calculated by assuming heat-transfer quantities based on previous experiments on similar nose shapes at these flight conditions and using a method of finite differences to determine the heat flow into the wall. Figure 20 presents time histories of the surface temperature which were calculated at two locations on the nose of model B. Because of the much greater heat capacity of the copper nose used on model B, these calculated temperatures are much lower than the temperatures on model A which were discussed previously.

Because of the extreme temperatures experienced on the nose of model A, it is reasonable to assume that structural failure was the cause of loss of telemeter signal. The heating calculated for model B was not so severe at the time the telemeter signal was lost; however, in these calculations laminar-flow heat-transfer quantities and zero angle of attack were assumed. If these conditions were different the heating may have been much worse and the copper nose may have weakened sufficiently to fail. Thus, the loss of telemeter signal from model B may also have been the result of structural failure caused by heating.

RESULTS AND DISCUSSION

Comparison of Measured and Theoretical

Received Signal Strengths

Time histories of the received signal strength and the signal strength calculated in accordance with free-space theory are presented in figures 21 and 22 for models A and B, respectively. Data are presented only for the time following fourth-stage firing since this time covers the period of significant heating of the gases surrounding the models and includes speeds above a Mach number of 5.0 for both models. In figures 21 and 22 the signal strength is not shown at the time of fourth-stage and fifth-stage rocket firing. At these times variations in signal strength were on the order of 20 to 30 decibels. It is thought that these large variations were caused either by reflections during separation of the stages or by transient changes in the attitude of the model which placed the receiving site in a different position in the antenna pattern; or by some combination of these items.

In figure 22, the large difference between the measured and theoretical signal strengths for model B is thought to have been caused by low power-supply voltage in the model. This model was delayed during the launching procedure and remained on its internal battery supply much longer than was desired. Measurement of the signal strength with the model on the launcher showed that the received power was 12 decibels below that of model A and that this power was decreasing slowly at the time of firing. However, it is estimated that the decrease in power because of supply-voltage changes during the time interval covered in figure 22 was less than 2 decibels.

Changes in Signal Strength at Increased

Velocity Flight Conditions

Direct comparison between the measured and theoretical plots in figures 21 and 22 is of limited value because of the difficulty in predicting the signal strength by using free-space-propagation theory alone. Factors such as multipath transmission and variations in atmospheric conditions could cause significant differences between the theoretical and measured signal strengths. For this reason, it appears that the most significant information is in the changes in signal strength during each flight. It is recognized that the factors mentioned previously may also affect these changes in signal strength; however, for these flights the part of the transmission path in the lower atmosphere is essentially constant, and atmospheric conditions should remain unchanged during the short time interval required for each test.

In order to indicate the attenuation experienced at increased velocity flight conditions, the changes in measured signal strength were corrected by the amount predicted by using free space theory. A time following fourth-stage ignition was selected as the reference point, and the changes in both the measured and theoretical received signal strength were determined until the time the telemeter signal was lost. The difference between the measured and the theoretical changes in signal strength then gives the change in signal strength which may be attributed to increased velocities. The resulting time histories, along with time histories of Mach number and altitude, are presented in figures 23 and 24 for models A and B, respectively.

In figure 23, it should be noted that a decrease in signal strength of approximately 9 decibels occurred between 89.0 seconds and 90.0 seconds, and that this decrease was recovered after fifth-stage ignition and separation of the fourth and fifth stages. The continuous decrease in signal strength following fifth-stage ignition may have been the result of thermal ionization in the gases surrounding the model or other conditions existing at increased flight velocities. However, study of the measured transverse accelerations indicated that the model reached an angle of attack of 10° at the time at which the telemeter signal was lost. This change, or a change in attitude during structural failure, may have placed the receiving site in an unfavorable part of the model antenna pattern, resulting in decreased signal strength.

In figure 24, a decrease in signal strength occurred during fourth-stage burning at approximately the same time after ignition as was noted for model A. The signal strength continued to decrease after fifth-stage firing for model B and after 94.0 seconds the signal strength for

model B was approaching the thermal noise level of the receiver. Since no transverse acceleration measurements were made in model B, it was not possible to determine if the decrease in signal strength was related to possible attitude changes of the model.

Conditions at Increased Flight Velocities

Several aspects of the problem of radio transmission at increased flight velocities are as follows:

(1) Increased electron concentration in the flow field surrounding the model may cause attenuation and reflections of the radiated signal; also, impedance mismatch of the radiating antenna may occur with a resulting power loss.

(2) At increased concentrations of free electrons and ions, and with low local pressures, the electric field strength between parts of the radiating antenna may cause breakdown and power loss in arc discharge.

(3) During rocket ignition and burning, combustion products in the exhaust gases may produce additional attentuation if the signal path passes through these gases. At increased velocities and high altitudes, the expansion of the rocket exhaust gases will increase and a greater area is affected by these combustion products.

(4) Extreme heating present at increased velocities affects the properties of the dielectric material used in the radiating antenna. The dielectric-loss factor of this material increases and other changes may take place which reduce the radiated power.

(5) Natural atmospheric ionization and dissociation in the path between the transmitting antenna and the receiving site may be important during transmission from high altitudes. Since both models A and B were well below the ionosphere, this factor was not considered for the tests reported herein.

The factors listed as items (1) and (2) are related to the physical structure of the gases surrounding the model. Detailed analysis of the interaction between these gases and the electromagnetic field is an extremely difficult problem which requires information that is not available.

Rocket combustion products may have resulted in some attenuation. This possibility is indicated in figure 23 by the recovery of signal after fourth-stage burnout and following separation of the fifth stage.

It is significant that the thermal ionization due to increased velocity
should have been much greater at 90.8 seconds than at 89.8 seconds, yet
the signal strength increased approximately 6.0 decibels. The results
shown in figure 24 for model B do not agree with this; however, it
should be noted from figures 12 and 13 that the transmission path for
model B is at a much greater angle off the longitudinal axis than for
model A. It is reasonable to expect that the effects of the combustion
products were greatly reduced at this increased angle.

Estimates of the heating experienced by the aluminum oxide antenna
dielectric material (Coors Porcelain Co. type AI-200) showed that sur-
face temperatures of 930° F and 500° F were reached for models A and B,
respectively. Information on the properties of this material is not
available at the operating frequency of 219.5 megacycles. However, at
a frequency of 1×10^6 cycles the dielectric-loss increases from 0.0267
at 68° F to 0.107 at 930° F; and at 1×10^{10} cycles the loss factor
increases from 0.0146 to 0.0179 over this temperature range. Qualita-
tive tests made by substituting a material whose dielectric-loss factor
was known to exceed that of aluminum oxide at elevated temperatures
indicated that the loss from this source was less than 3 decibels.

As was stated previously, analysis of the physical state of the
gases surrounding the models is difficult. However, from conductivity
considerations it is reasonable to assume that the resulting attenua-
tion is a function of the free-electron concentration at the radiating
antenna and in the flow field surrounding the model. In order to indi-
cate the conditions for these models and to provide comparison with a
practical case, calculations were made of the electron concentration at
the stagnation point for models A and B and for a hypothetical ballistic
missile during reentry.

It is necessary to emphasize that exact comparison of the trans-
mission from these models and the ballistic missile case cannot be made
on the basis of the electron concentration at the stagnation point
alone. Such comparison would require information on the electron con-
centration throughout the entire flow field surrounding the vehicles
and knowledge of the interaction with the electromagnetic field pro-
duced by the transmitting antenna. Thus a ballistic missile might have
more, or less, attenuation than these models even though the stagnation-
point electron concentrations are the same. However, the increased
electron concentration at the stagnation point with increased velocity
should be representative of increased electron concentration throughout
the flow field.

Figure 25 presents the free-electron concentration at the stagna-
tion point for models A and B, and for a reentry missile with $\dfrac{W}{C_D A}$ of

100 lb/sq ft, reentry altitude of 200,000 feet, reentry angle of -21.8°, and reentry velocity of 20,000 feet per second. These electron concentrations were calculated with the equilibrium composition of air given in reference 3 and the stagnation-point conditions in reference 4. Atmospheric density and temperature values for the ballistic-missile case were obtained from reference 5. It should be noted that both models A and B were flown at altitudes below the region of maximum electron concentration for the reentry missile; however, it is significant that the maximum electron concentration at which a telemeter signal was received approached the maximum electron concentration expected during reentry of such a missile.

CONCLUDING REMARKS

Two rocket-powered models were flown at hypersonic speeds with telemeters operating at a frequency of 219.5 megacycles. One model reached a Mach number of 15.5 at an altitude of 98,000 feet before the telemeter signal was lost, and the other model reached a Mach number of 15.7 at 70,500 feet. The reasons for loss of telemeter signal are not known; however, it appears that both models may have failed structurally because of severe aerodynamic heating at the time at which the telemeter signal was lost.

Analysis of the signal strength received from each model showed that significant decrease in signal strength occurred during the period of Mach number increase. It was not possible to determine the amount of attenuation caused by thermal ionization in the high-temperature gases surrounding the models or by other conditions experienced during the flights.

There is reasonable evidence, in one case, that part of the signal loss may have resulted from a change in model attitude which placed the receiving site in a null in the antenna radiation pattern. In this case it also appears that some attenuation may have been caused by rocket combustion products in the path between the model and the receiving site.

Increased losses in the antenna dielectric material at the elevated temperatures produced by aerodynamic heating probably caused only slight signal loss during the model flights.

It is important that successful telemeter transmission was obtained at these flight conditions even though there may have been considerable attenuation because of thermal ionization. Also, it should be noted that the maximum stagnation point electron concentrations at which a

telemeter signal was received closely approached the maximum concentration expected for a reentry vehicle with $\frac{W}{C_D A}$ of 100 (where W is weight, C_D is drag coefficient, and A is frontal area of the body), reentry altitude of 200,000 feet, reentry angle of $-21.8°$, and reentry velocity of 20,000 feet per second.

Langley Aeronautical Laboratory,
    National Advisory Committee for Aeronautics,
        Langley Field, Va., April 2, 1958.

REFERENCES

1. Bland, William M., Jr., Rumsey, Charles B., Lee, Dorothy B., and Kolenkiewicz, Ronald: Free-Flight Aerodynamic-Heating Data to a Mach Number of 15.5 on a Blunted Conical Nose With a Total Angle of 29°. NACA RM L57F28, 1957.

2. Bullington, Kenneth: Radio Propagation at Frequencies Above 30 Megacycles. Proc. I.R.E., vol. 35, no. 10, Oct. 1947, pp. 1122-1136.

3. Logan, J. G., Jr., and Treanor, C. E.: Tables of Thermodynamic Properties of Air From 3000° K to 10,000° K at Intervals of 100° K. Rep. No. BE-1007-A-3, Cornell Aero. Lab., Inc., Jan. 1957.

4. Feldman, Saul: Hypersonic Gas Dynamic Charts for Equilibrium Air. AVCO Res. Lab., Jan. 1957.

5. The Rocket Panel: Properties, Densities, and Temperatures in the Upper Atmosphere. Phys. Rev., vol. 88, Second ser., no. 5, Dec. 1, 1952, pp. 1027-1032.
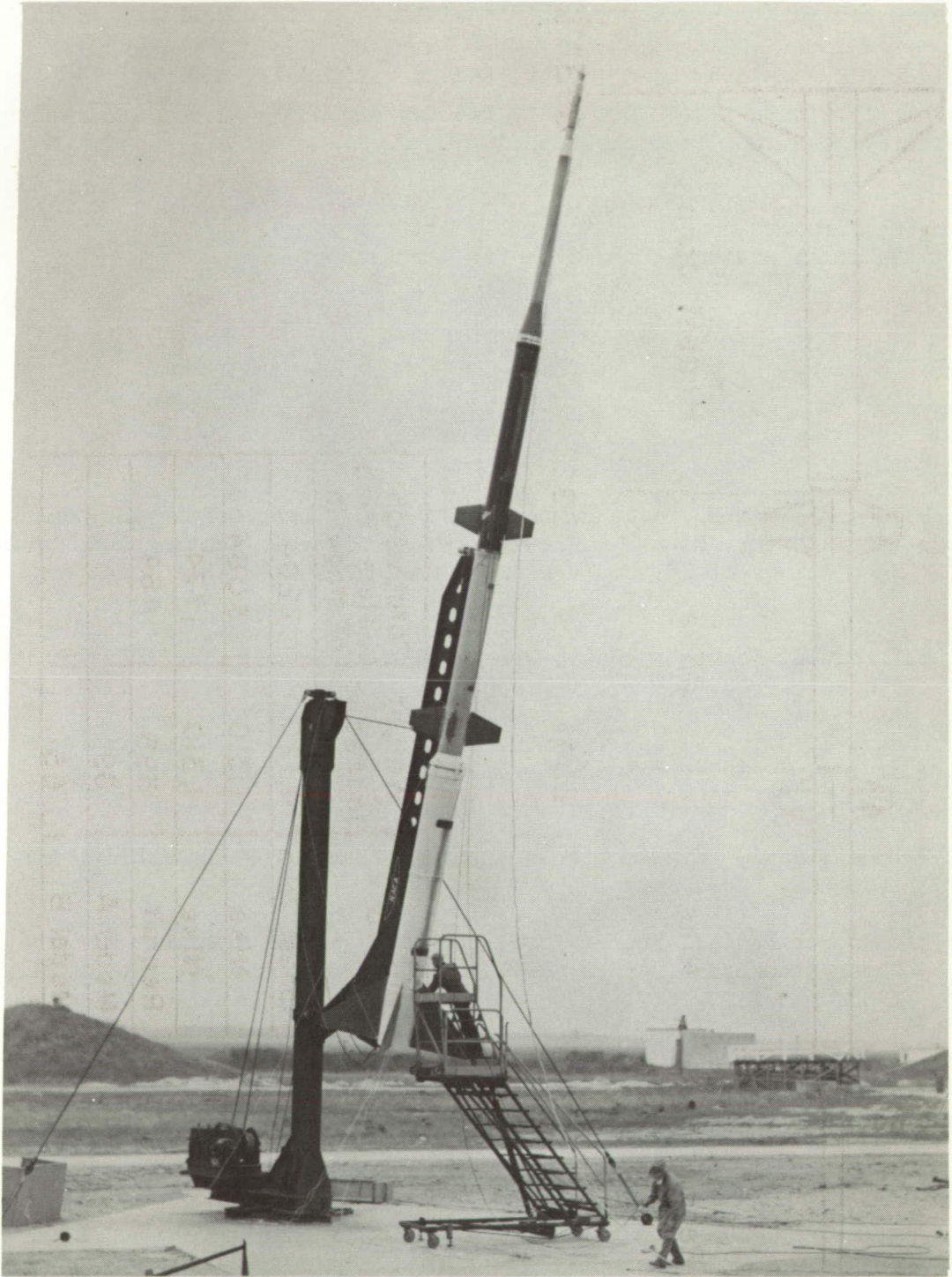
L-57-1085

Figure 1.- Photograph of five-stage rocket-powered model on launcher.
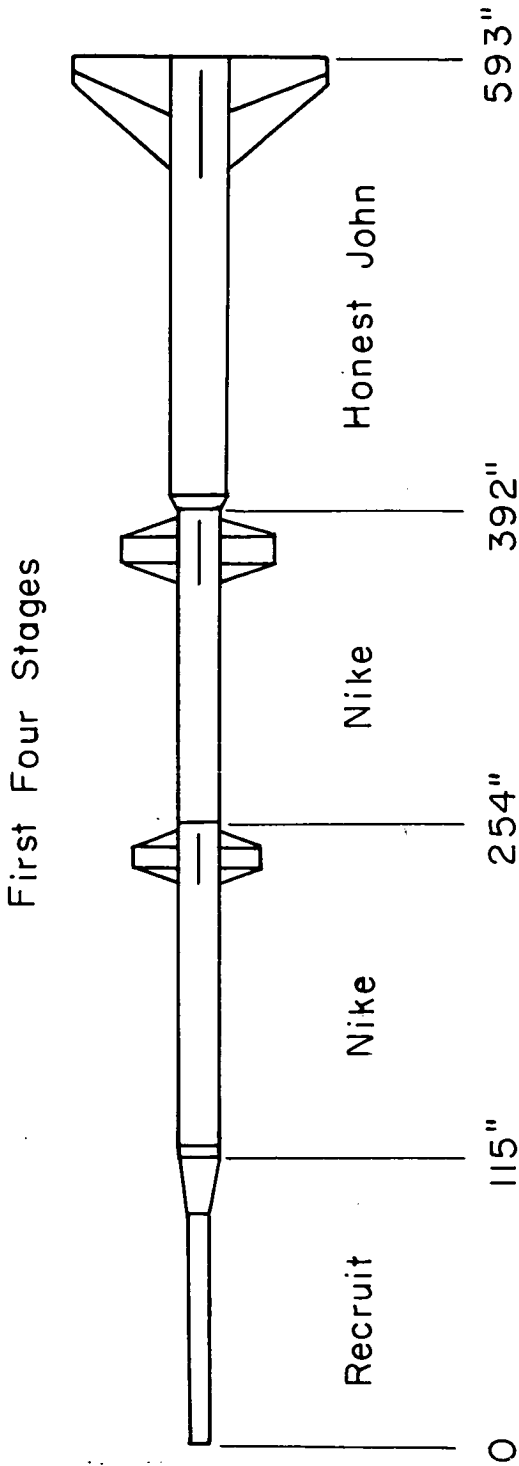
First Four Stages

Motor	Weight loaded, lb	Total weight before firing of stage, lb
Honest John	4,120	7204
Nike	1,310	3084
Nike	1,310	1774
Recruit	395	464
Model A	69	
Model B	65	

Figure 2.- Sketch of first stages and weights of components.
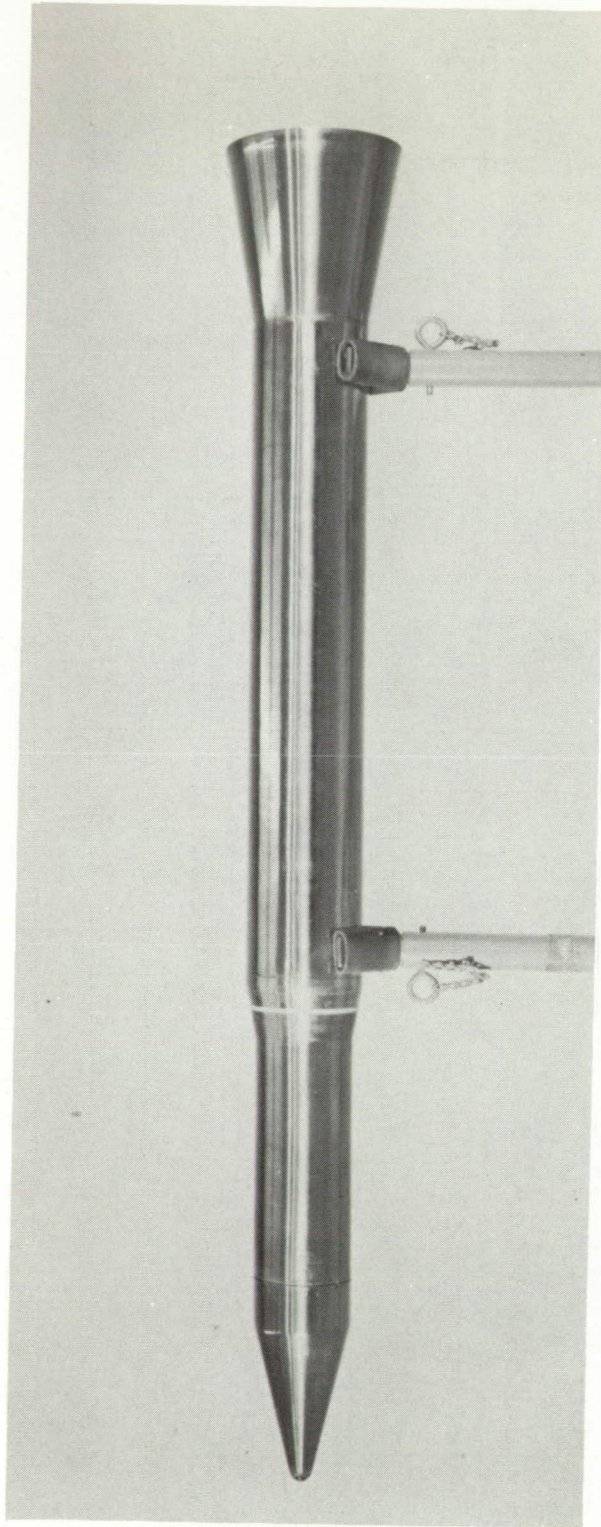
Figure 3.- Photograph of model A. L-57-1010
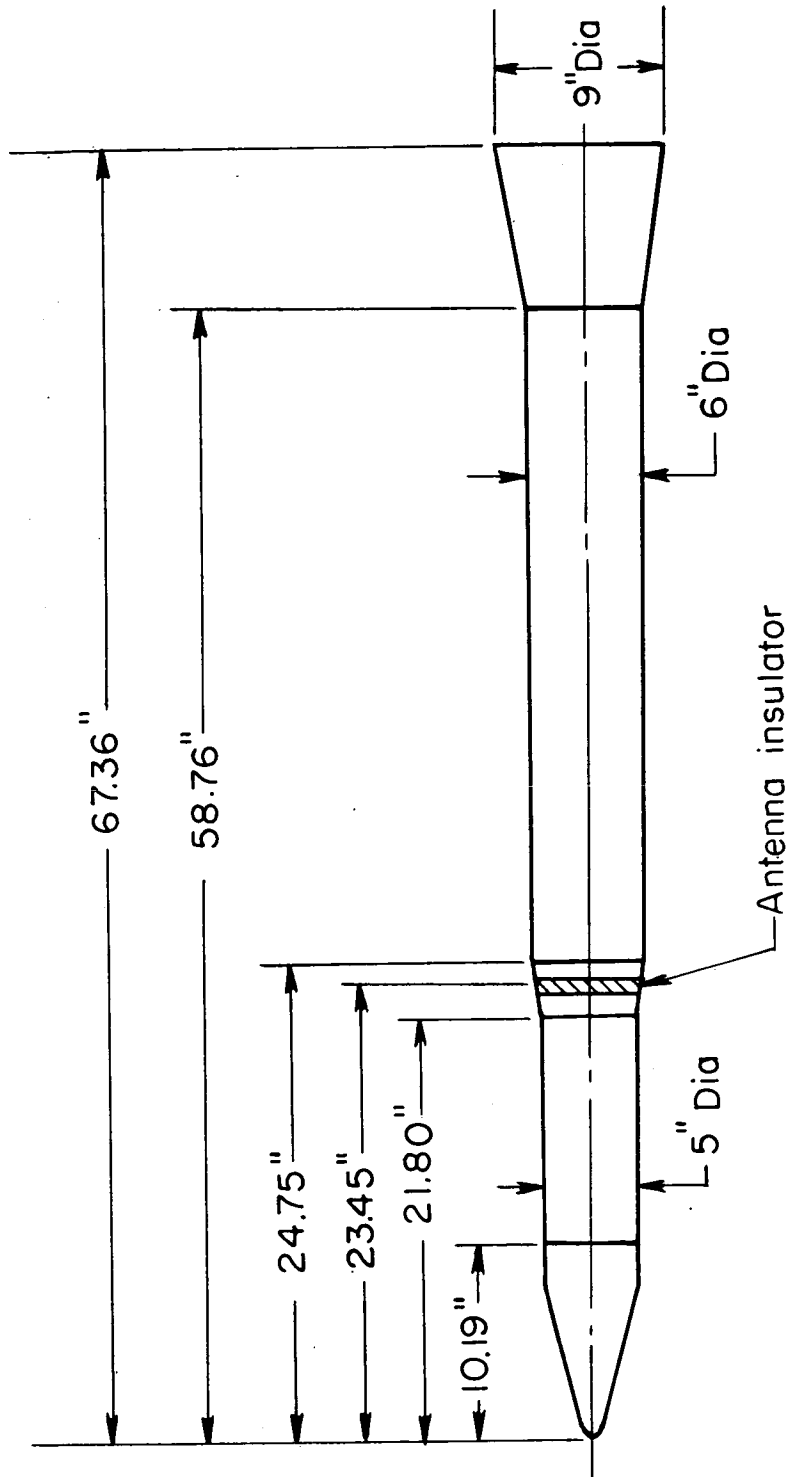
Figure 4.- Sketch of model A.
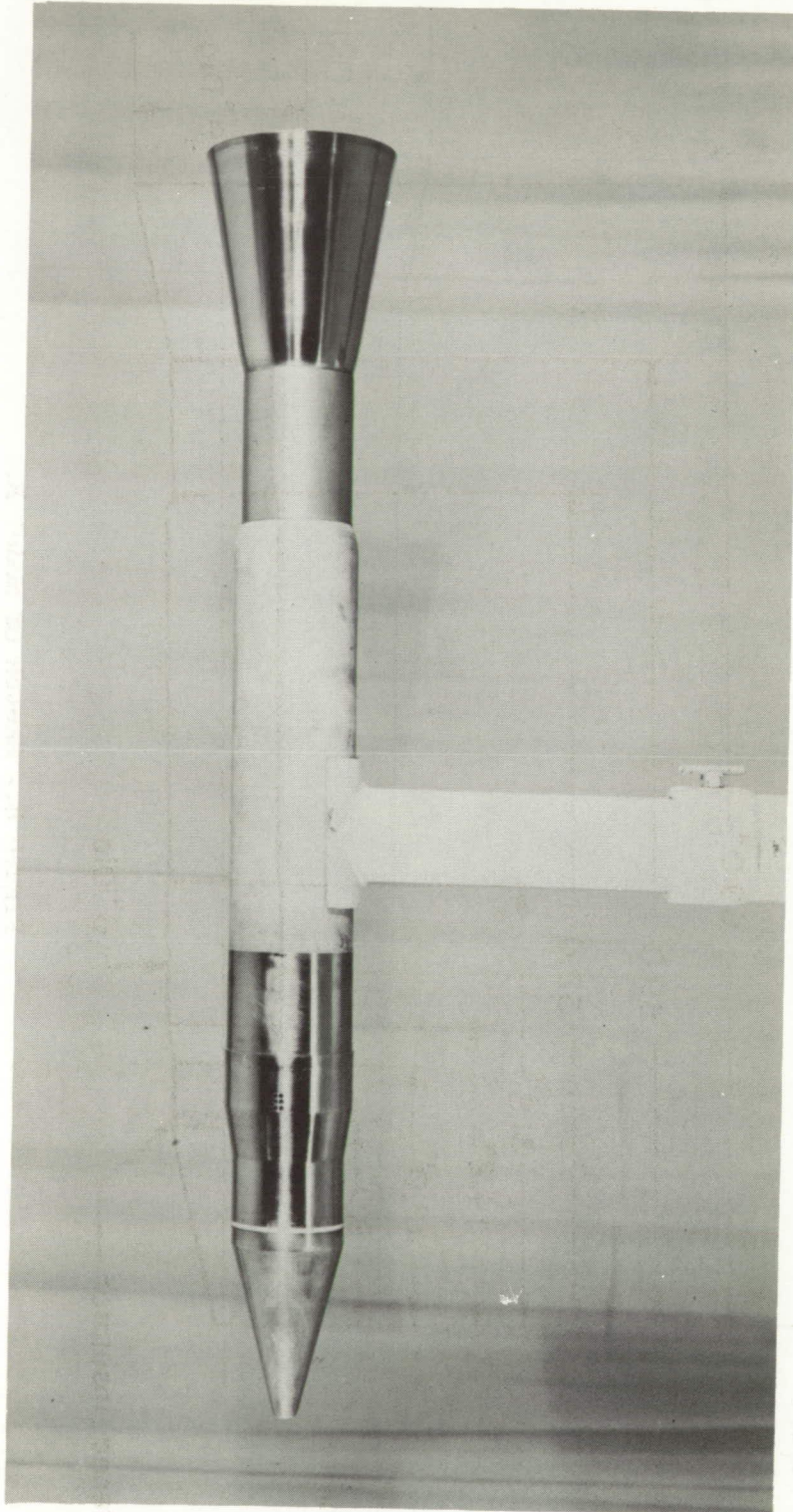
Figure 5.- Photograph of model B.   L-57-1087
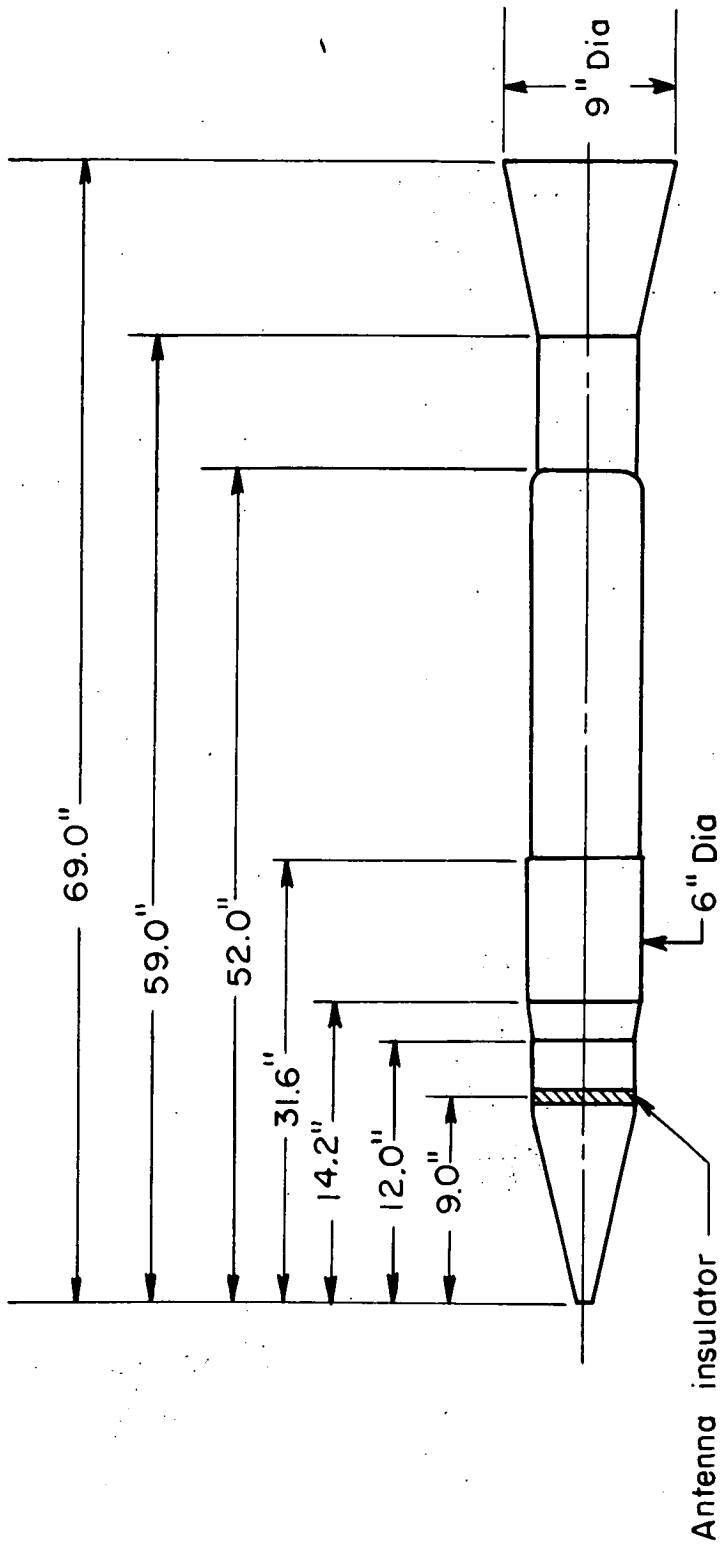
Figure 6.- Sketch of model B.

Lateral accelerometers

Longitudinal accelerometers

Inner insulating ring (micarta)

Outer insulating ring (aluminum oxide)

Insulating plug (micarta)

A

A

Shorting screws located approximately 180° from antenna feed point To short across inner insulating ring.

Shorting element

Insulating ring

Coaxial feed   cable

Antenna feed point

Section A-A
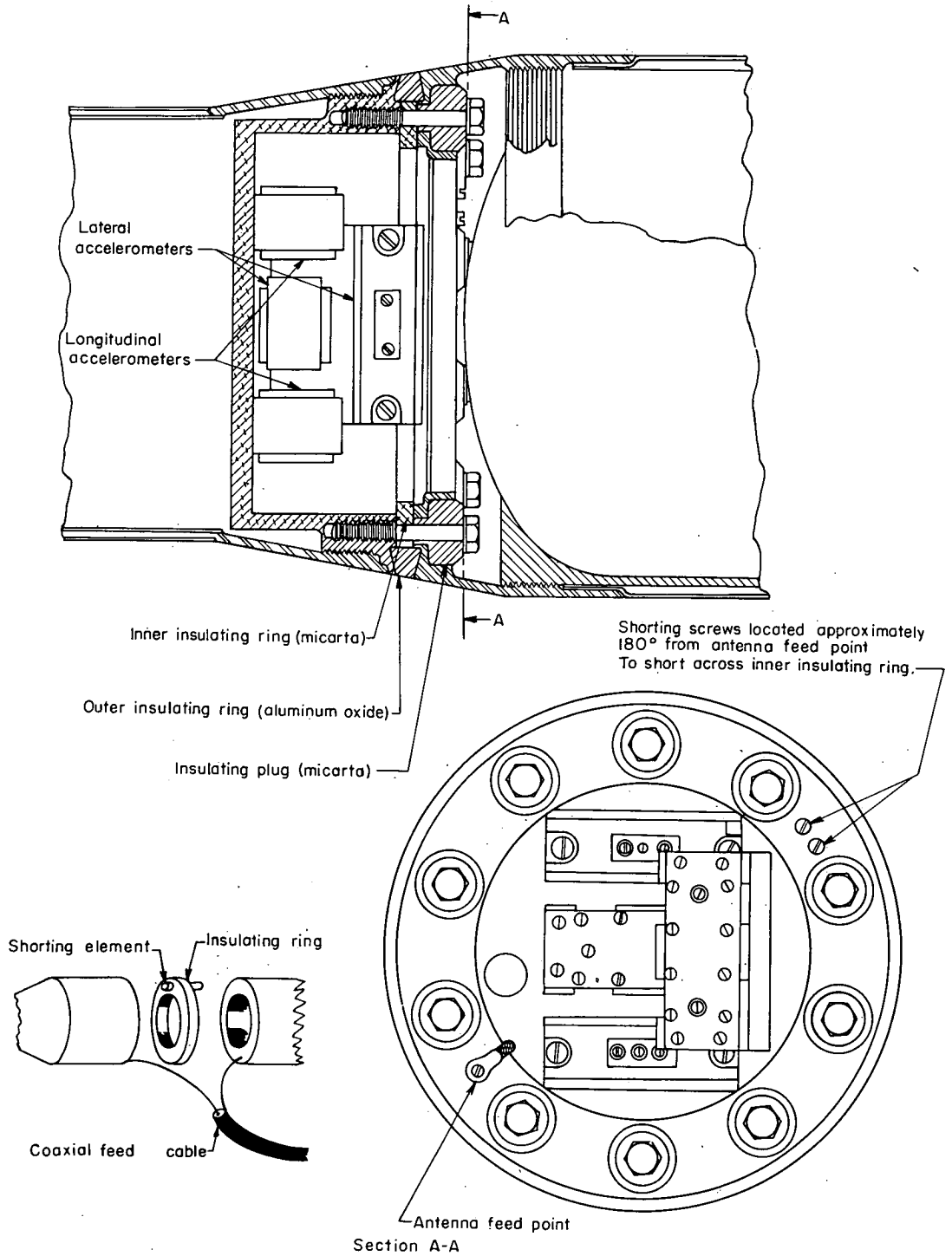
Figure 7.- Details of antenna construction of model A.
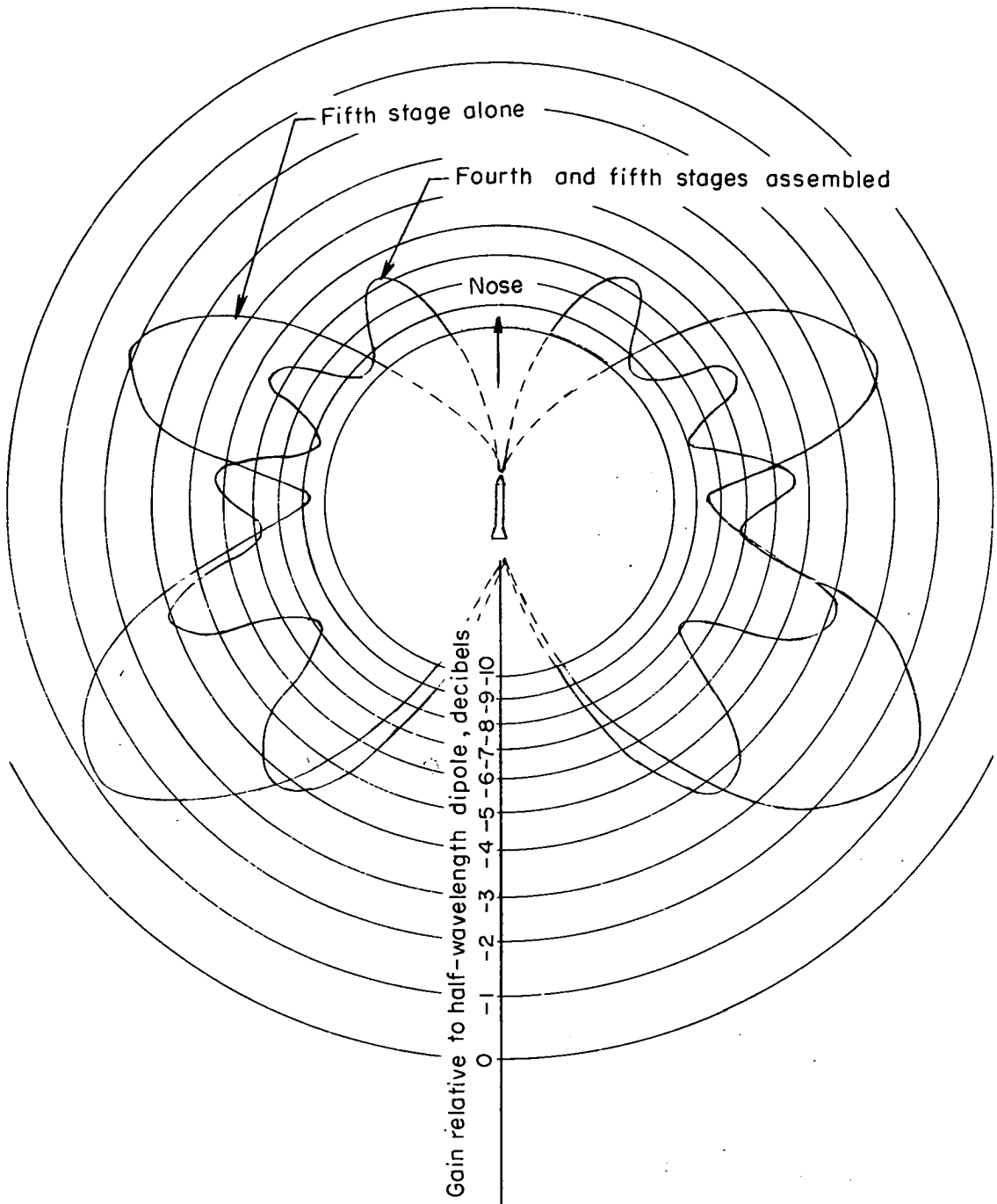
Figure 8.- Nominal antenna radiation patterns in plane containing longitudinal axis of model. Model A.

Insulating sleeve (micarta)

Inner insulating ring (micarta)

Outer insulating ring (aluminum oxide)

Shorting screws-located across
from antenna feed point. To
short across inner insulating ring.

Shorting element

Insulating ring

Coaxial feed   cable

Antenna feed point.

Section A-A
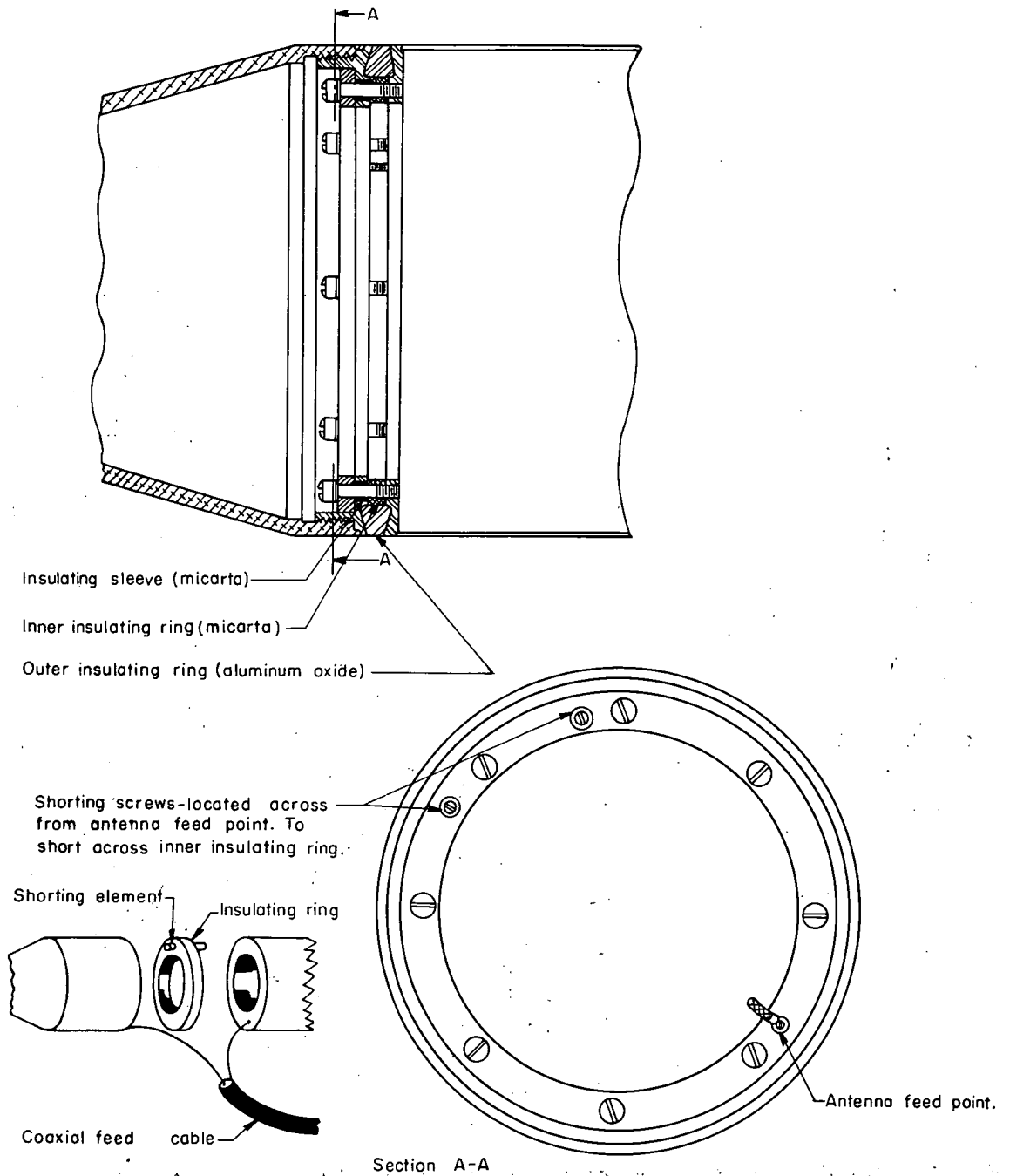
Figure 9.- Details of antenna construction of model B.
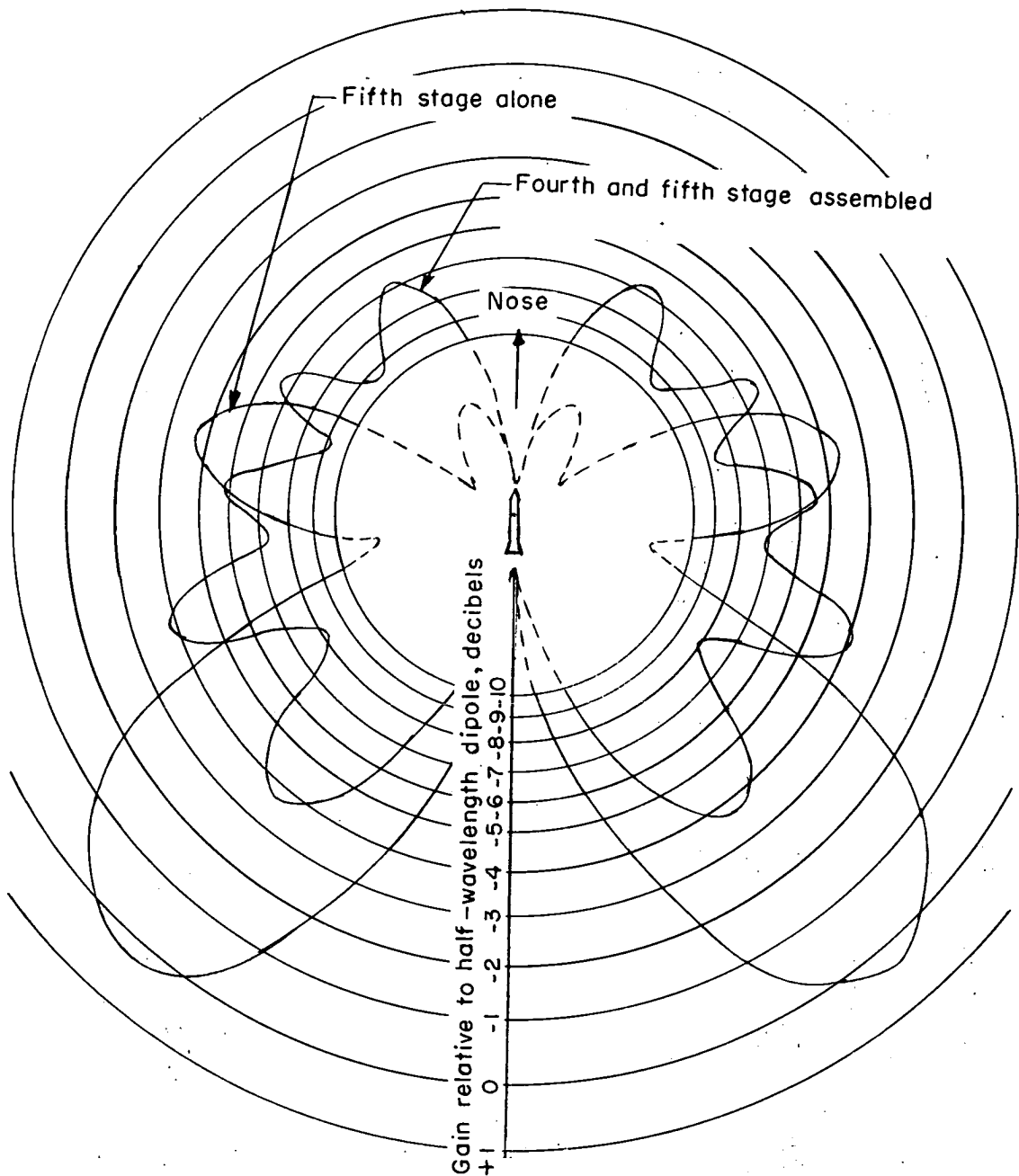
Figure 10.- Nominal antenna radiation patterns in plane containing longitudinal axis of model.   Model B.
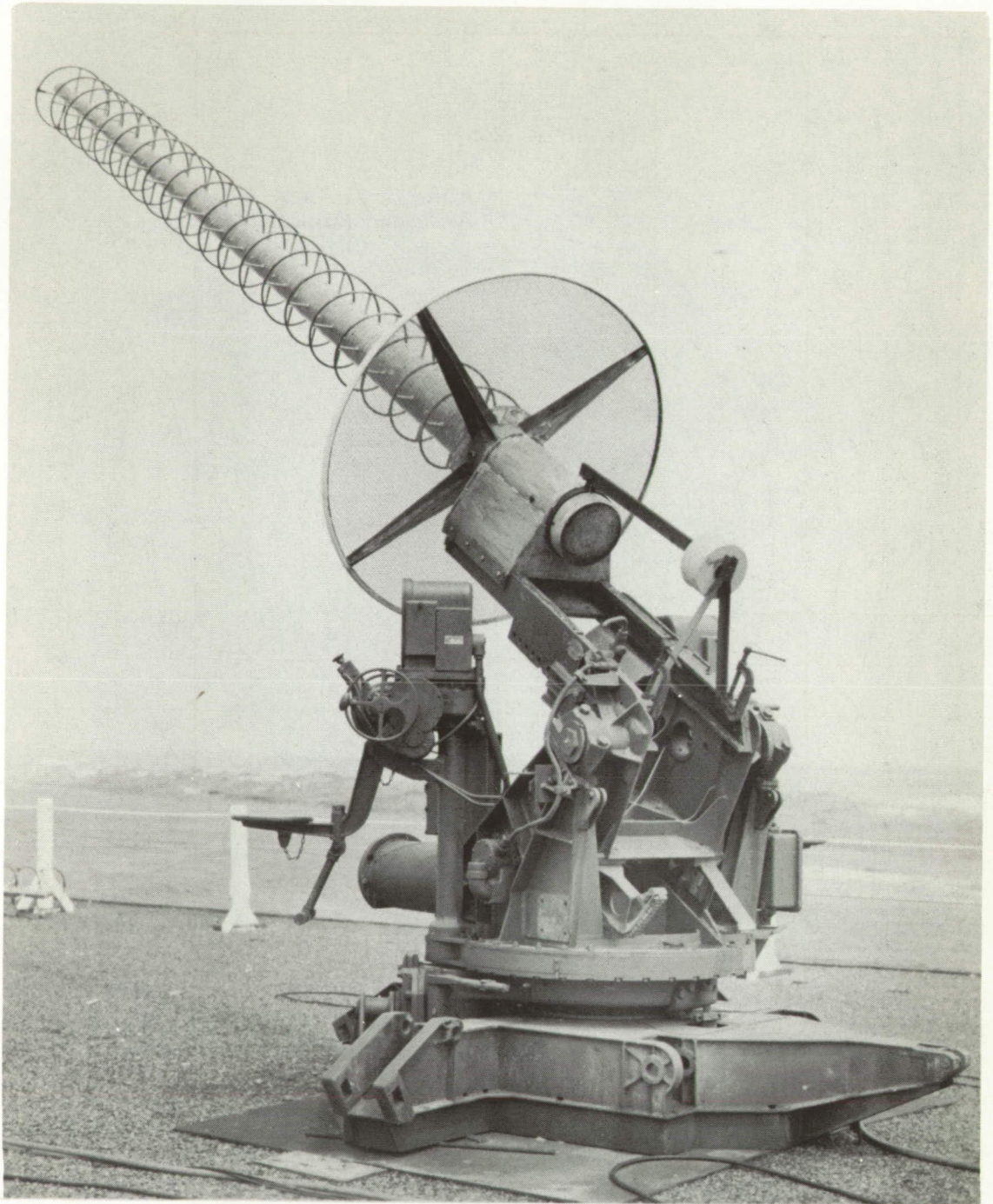
L-57-3664

Figure 11.- Photograph of telemeter receiving antenna.
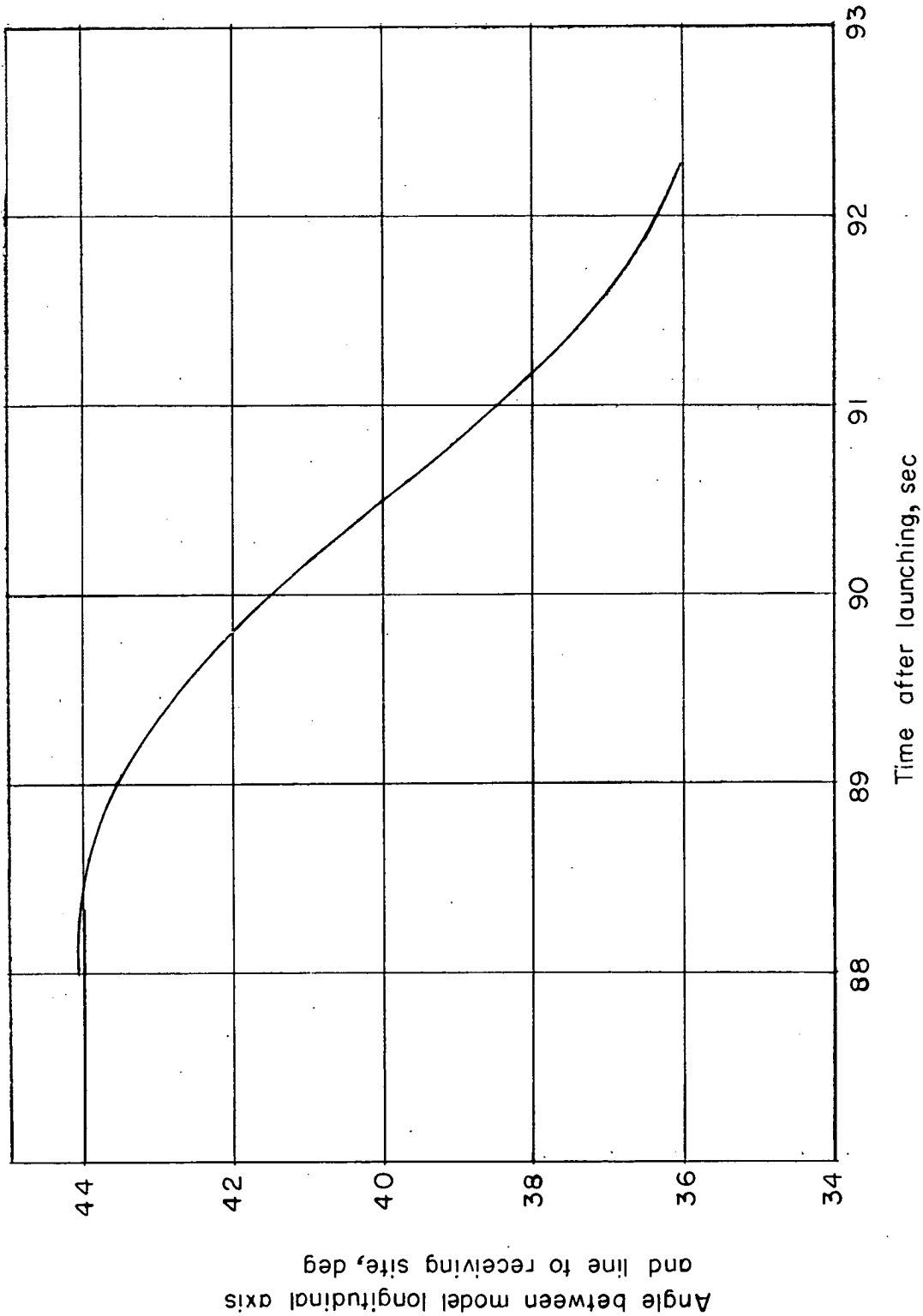
Figure 12.- Angular location of receiving site off longitudinal axis of model A.
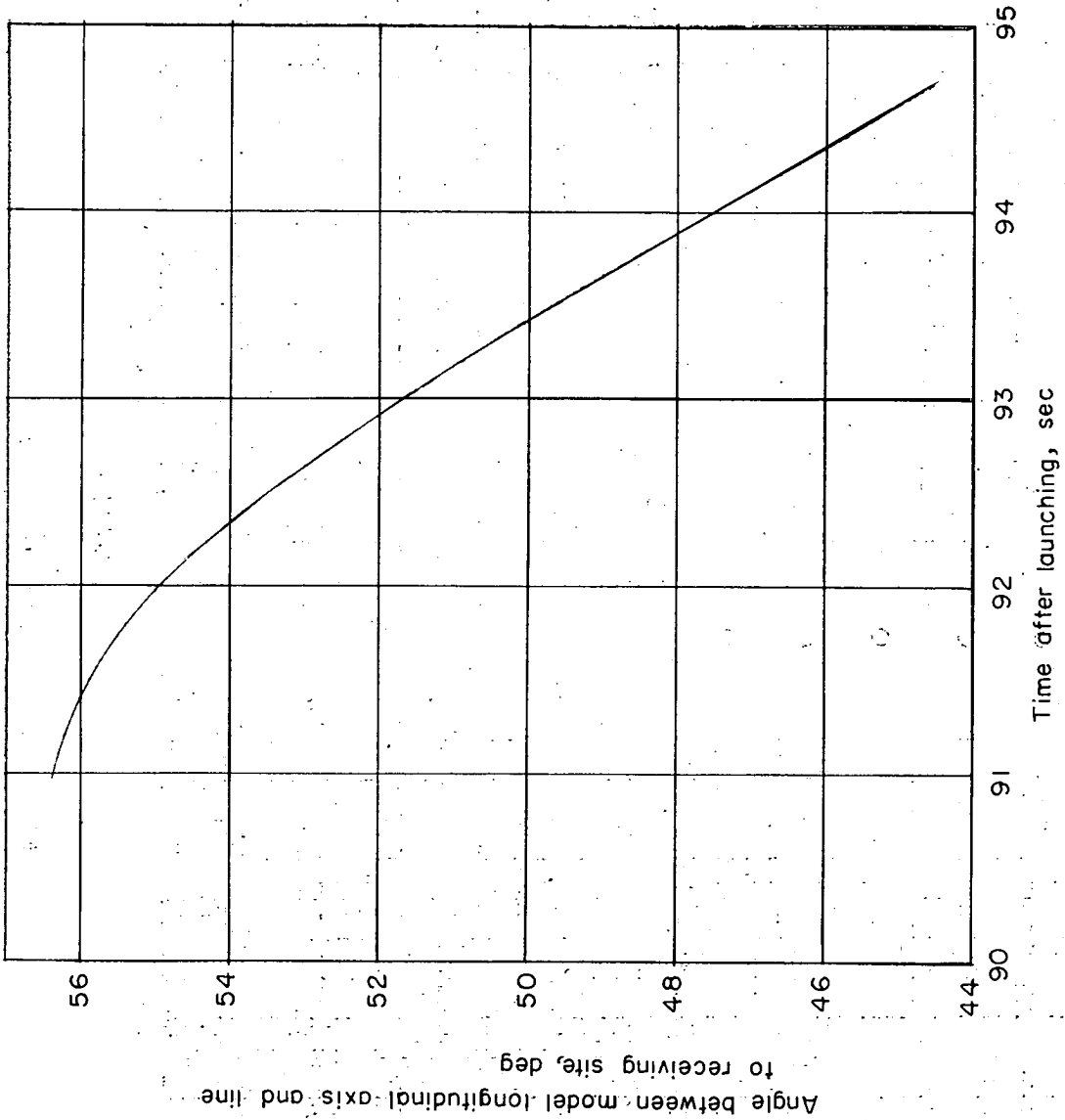
Figure 13.- Angular location of receiving site off longitudinal axis of model B.
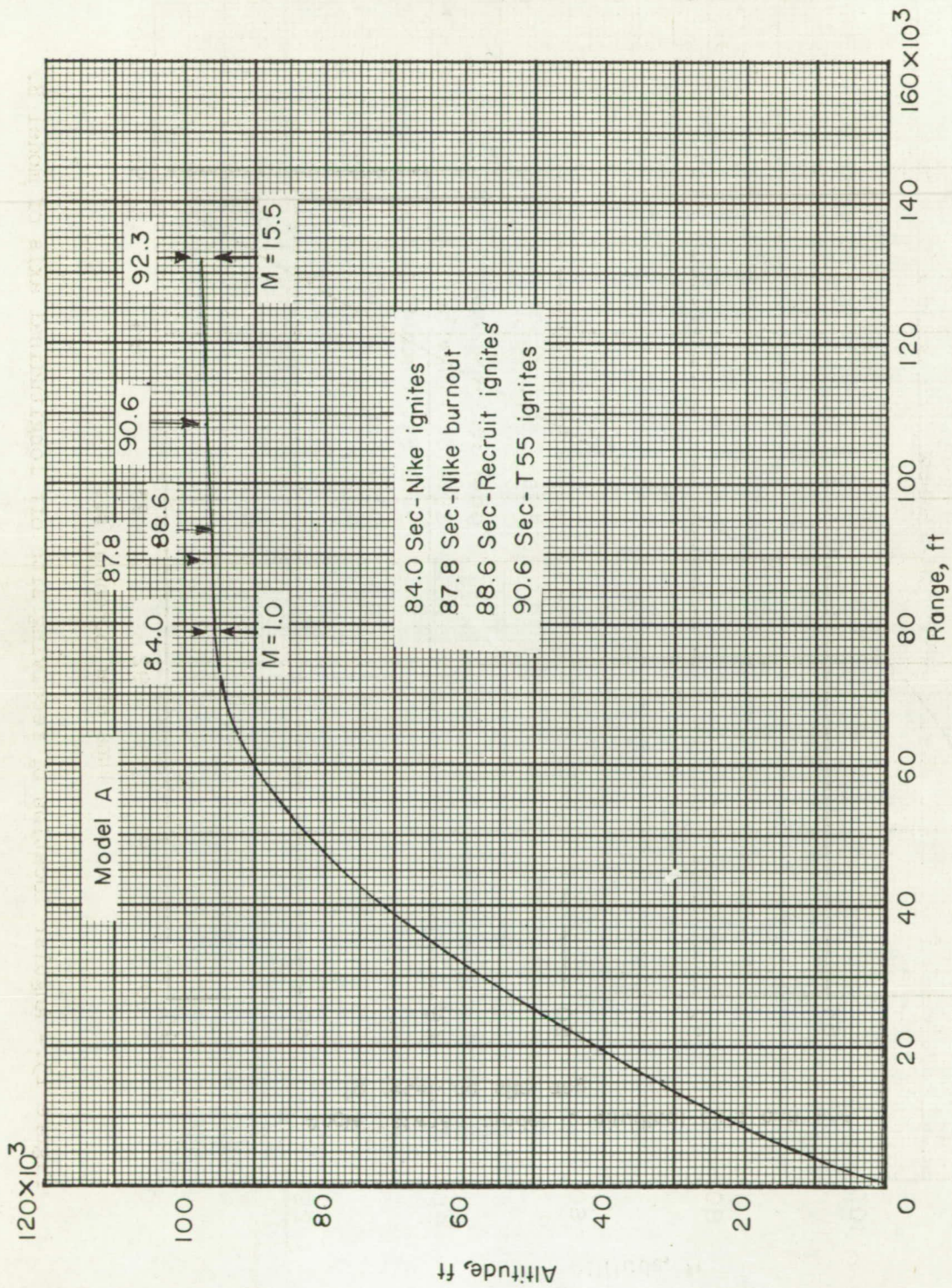
Figure 14.- Trajectory of model A.
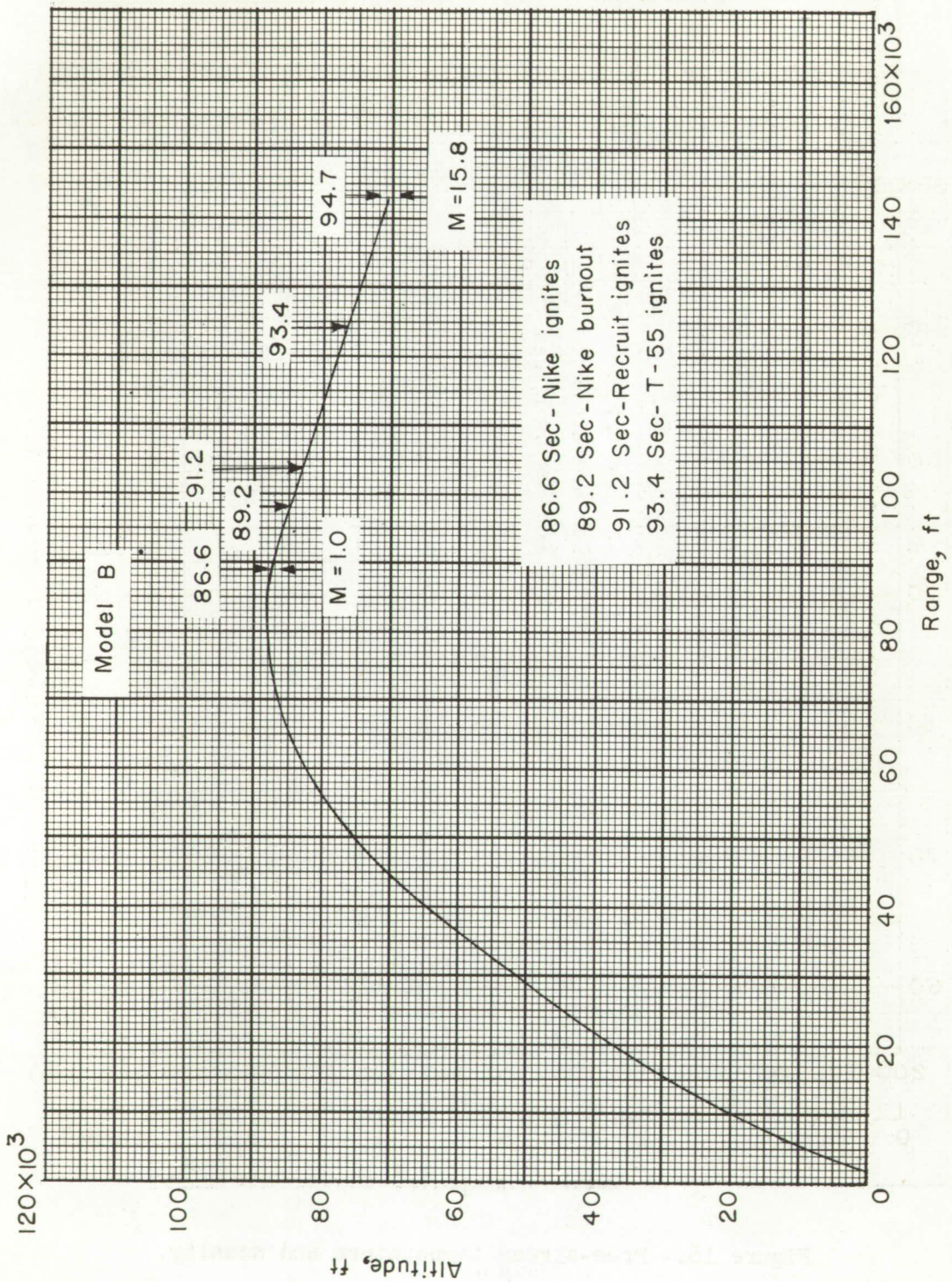
Figure 15.- Trajectory of model B.
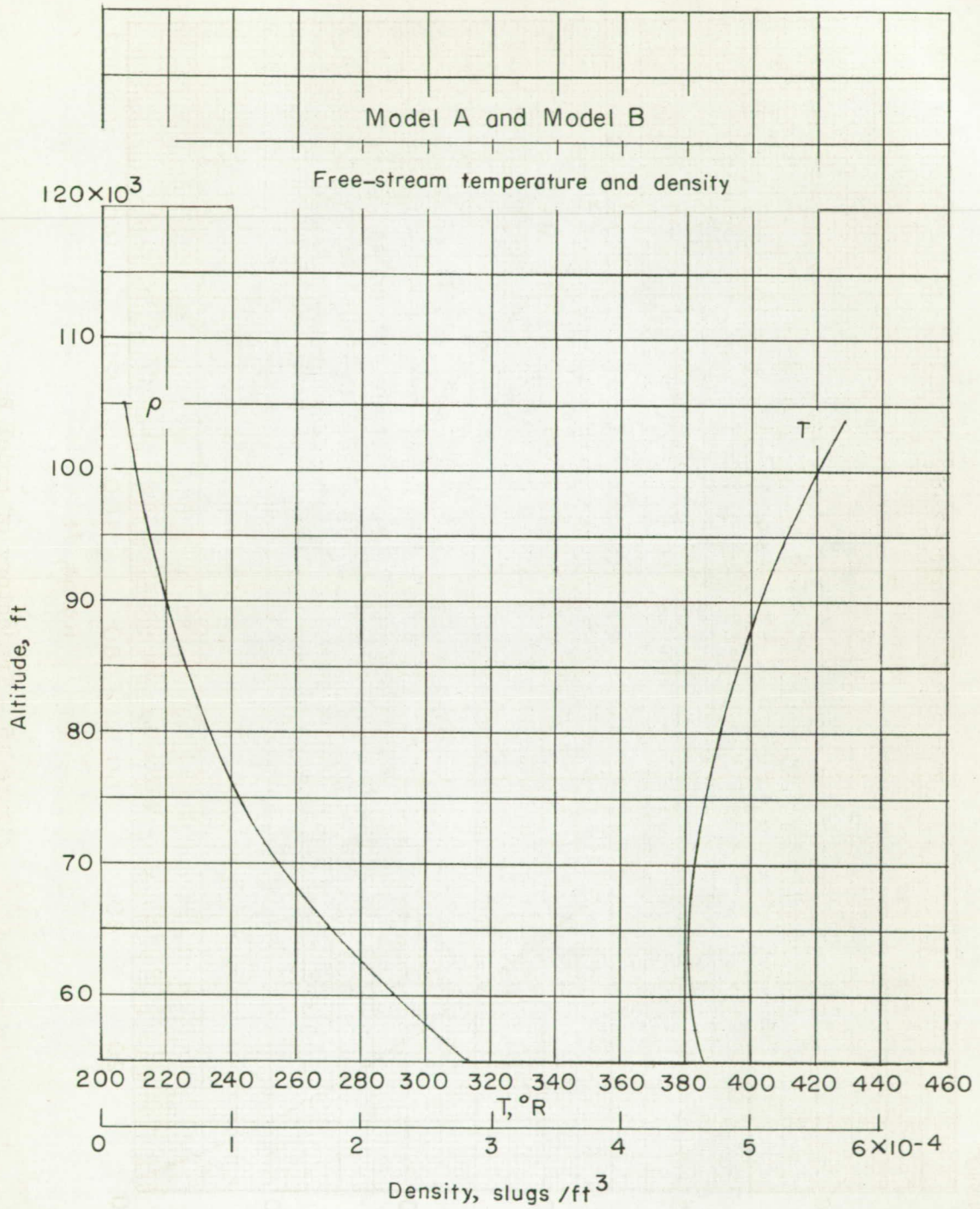
Figure 16.- Free-stream temperature and density.
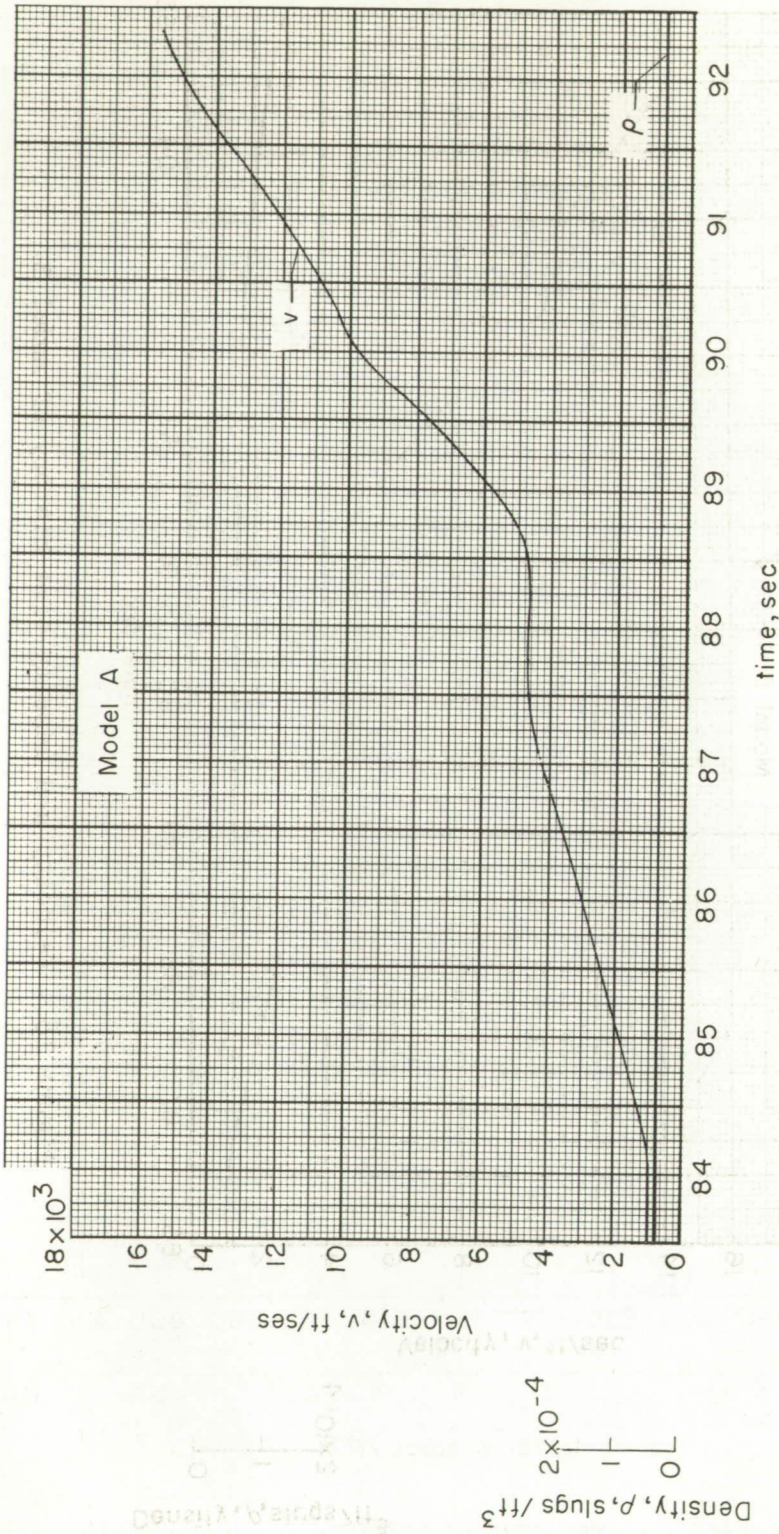
Figure 17.- Velocity and density time history of model A.
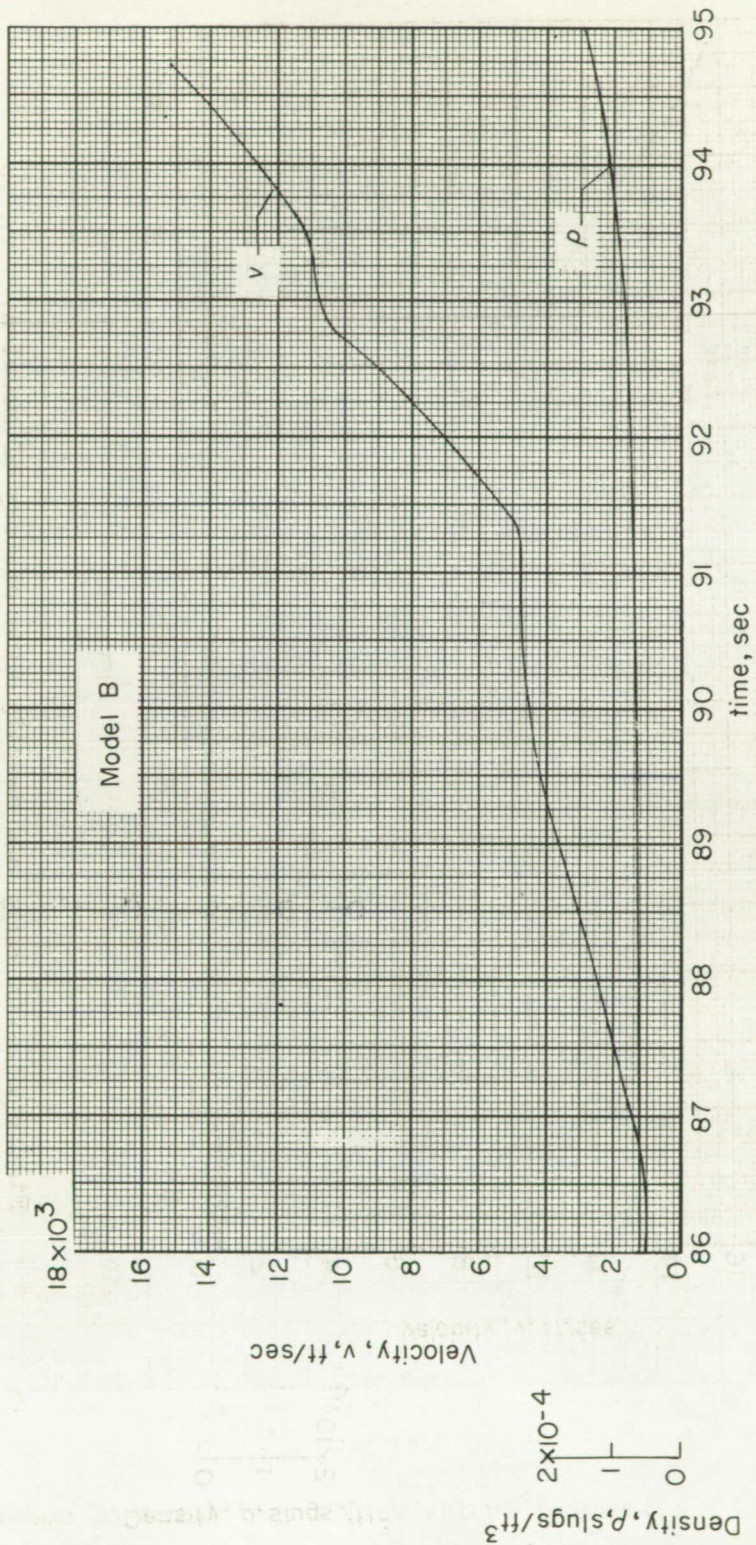
Figure 18.- Velocity and density time history of model B.
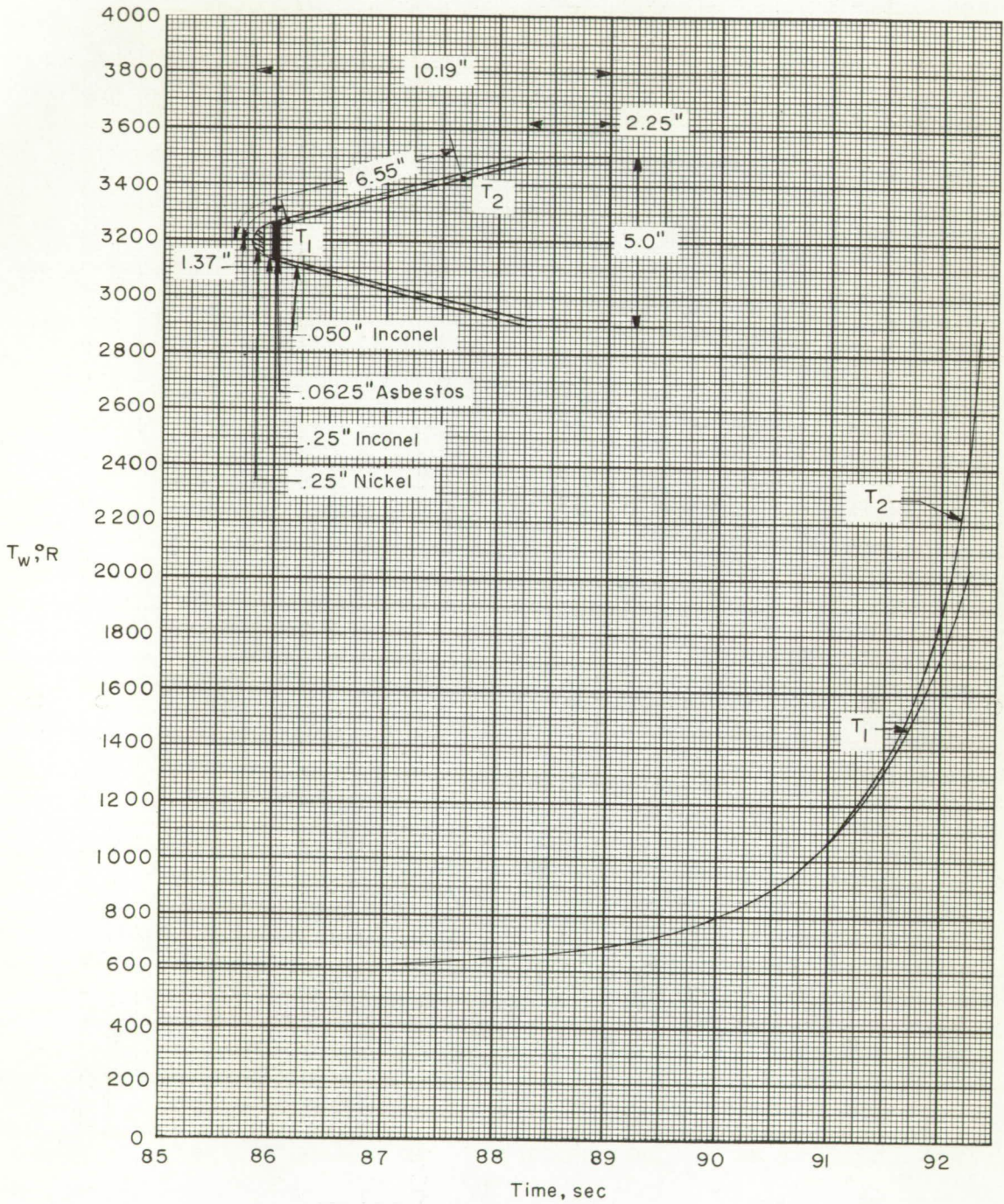
Figure 19.- Measured inside wall temperatures of model A.
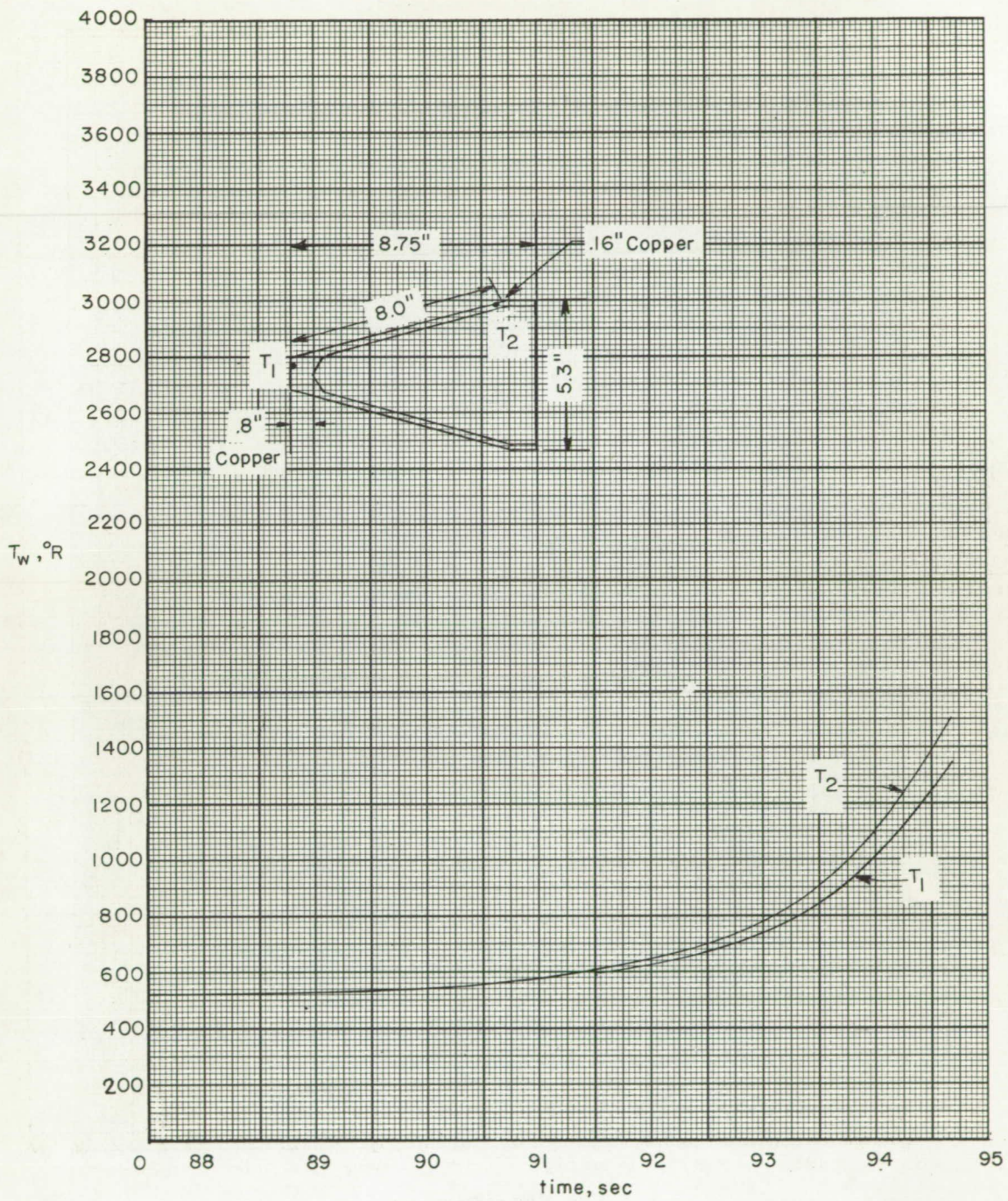
Figure 20.- Calculated outside wall temperature of model B.
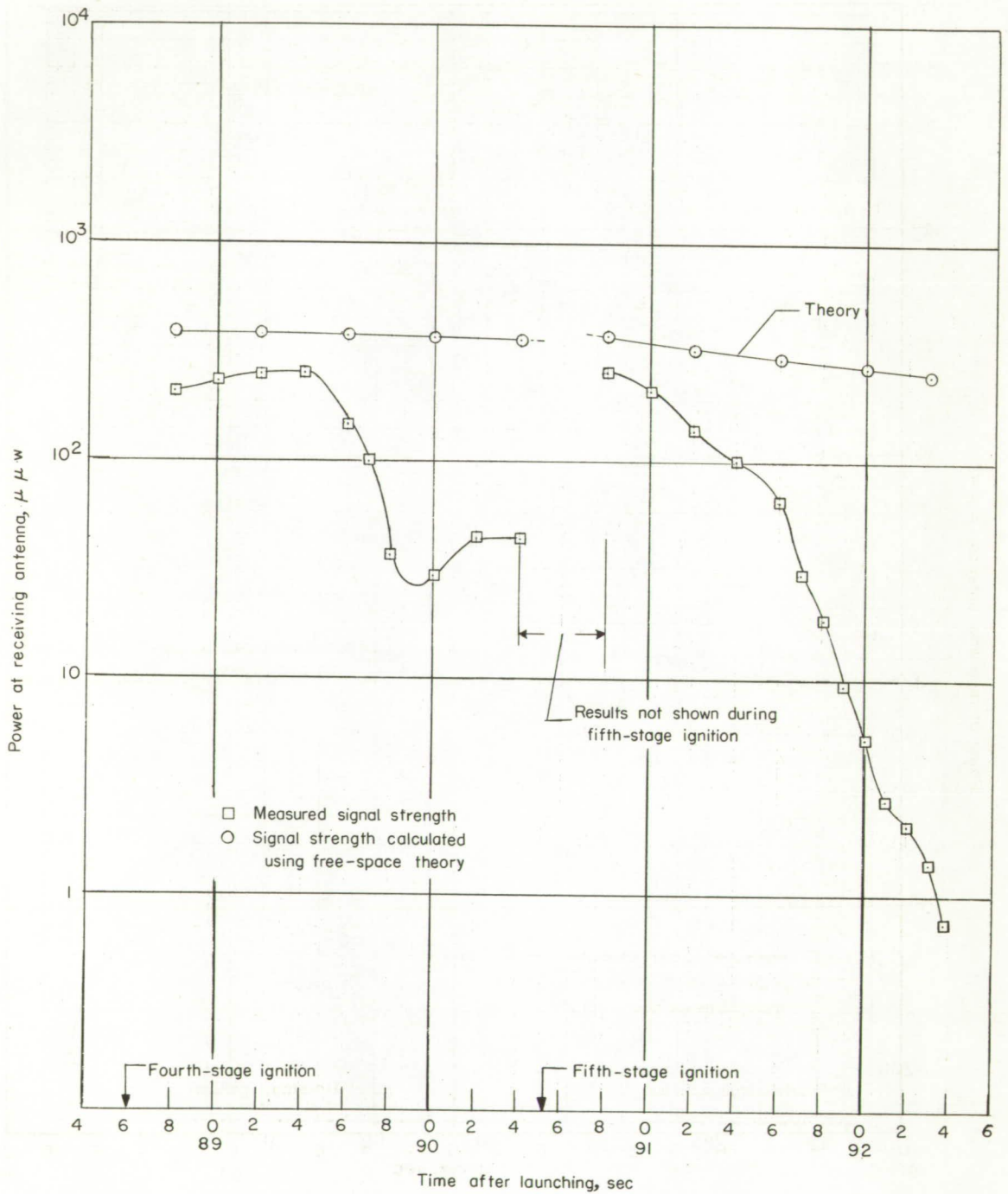
Figure 21.- Measured and theoretical received signal strength from model A.
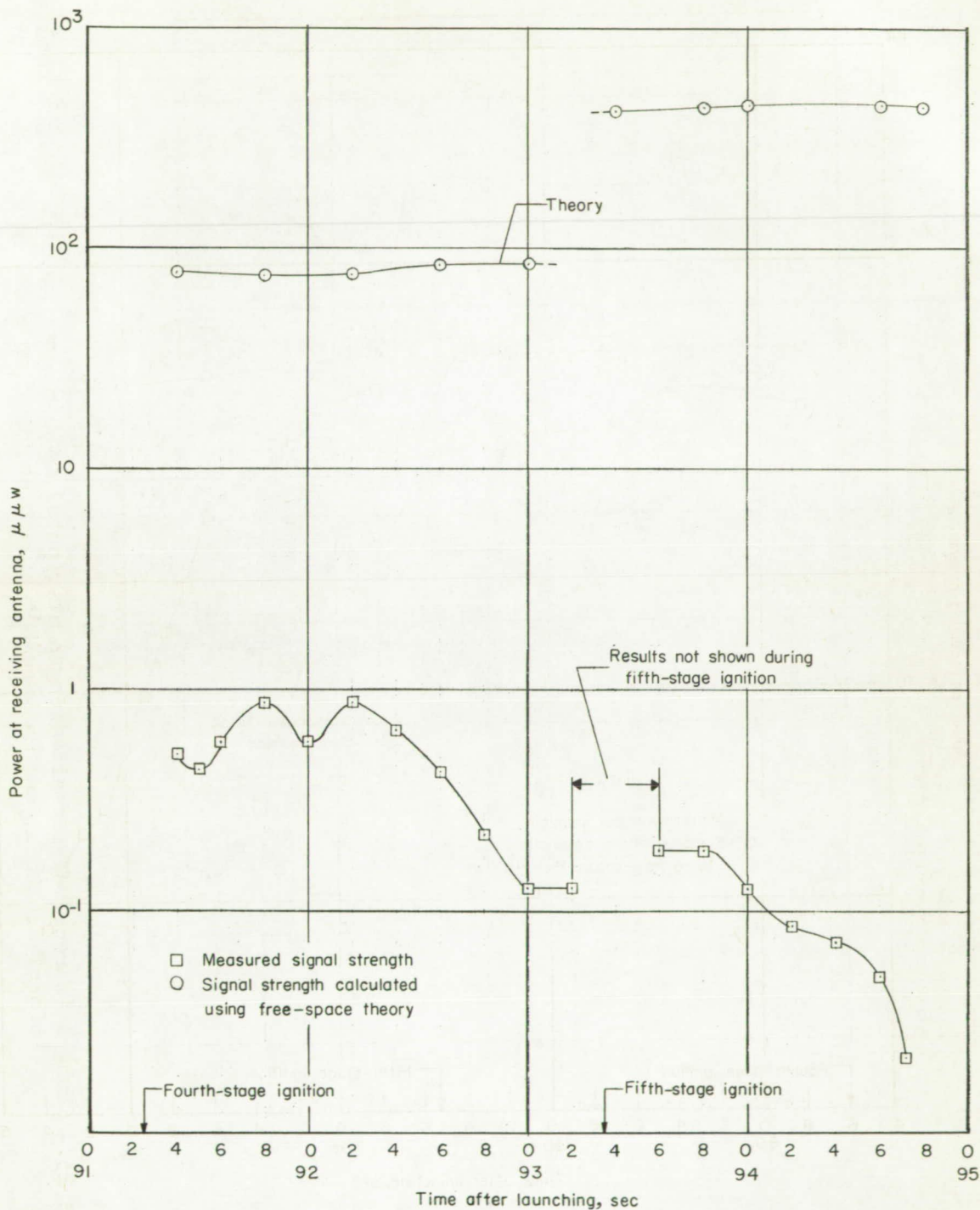
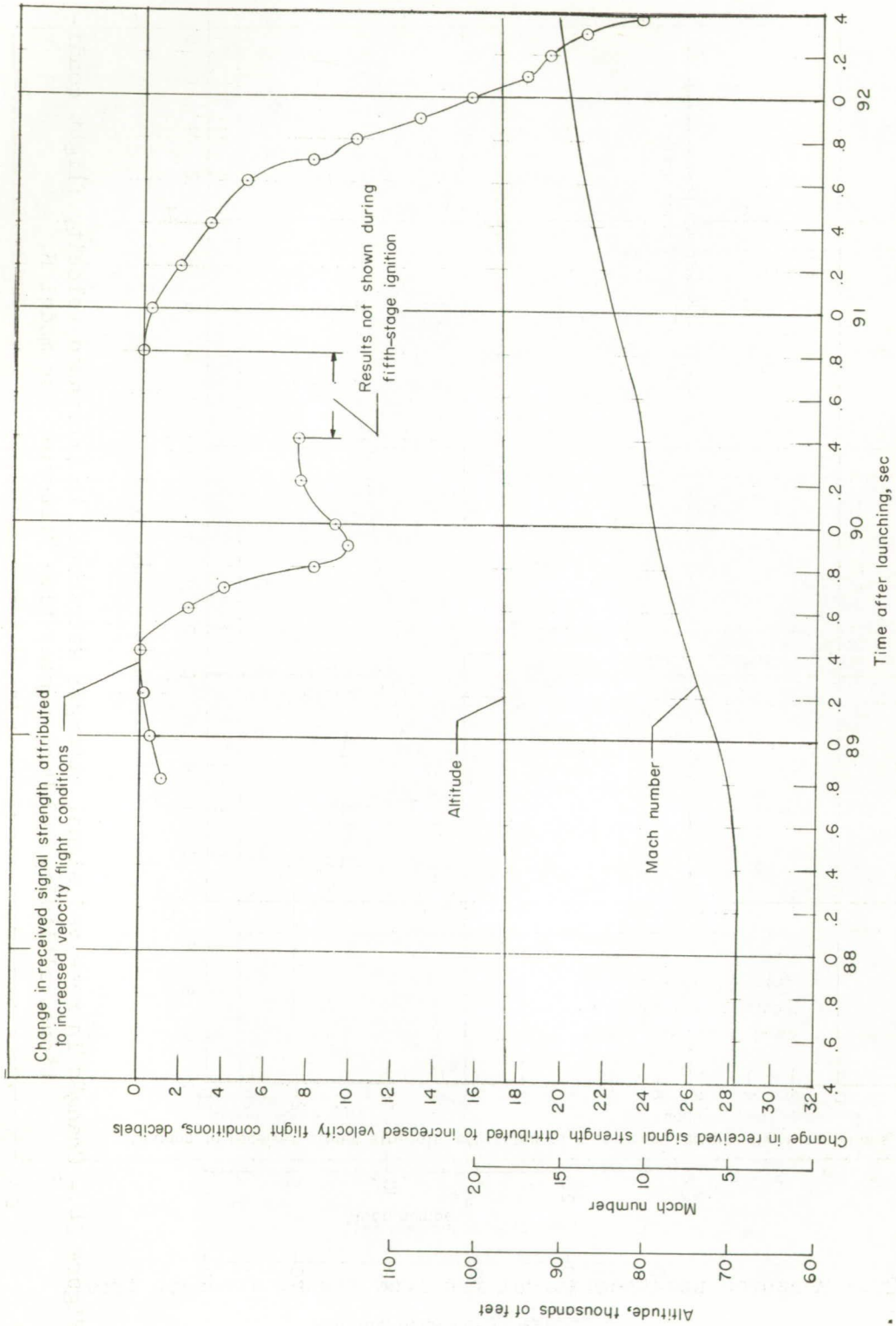Figure 22.- Measured and theoretical received signal strength from
model B.

Figure 23.- Changes in received signal strength attributed to increased velocity flight conditions, altitude, and Mach number time histories for model A.
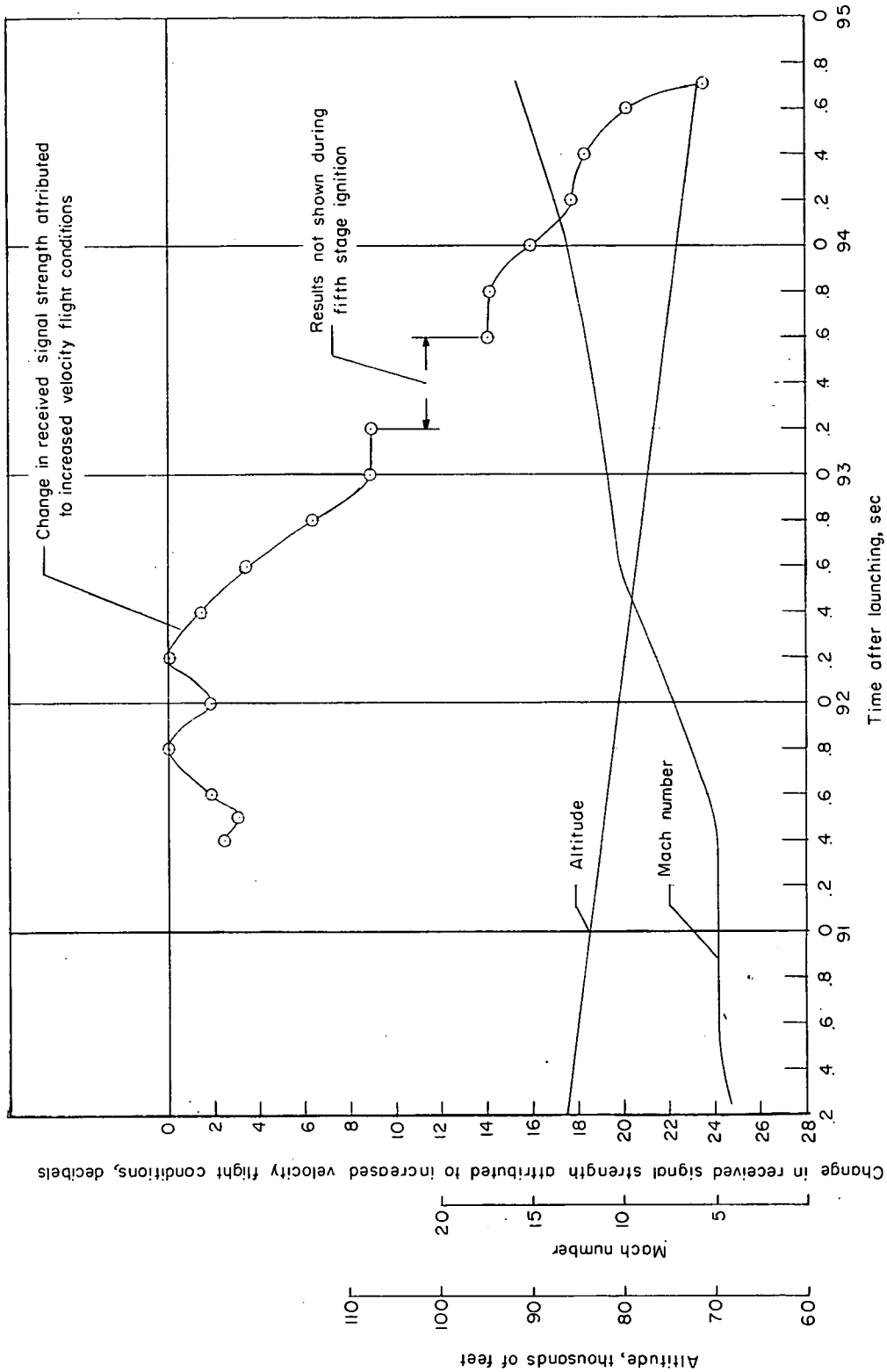
Figure 24.- Changes in received signal strength attributed to increased velocity flight condi-
tions, altitude, and Mach number time histories for model B.
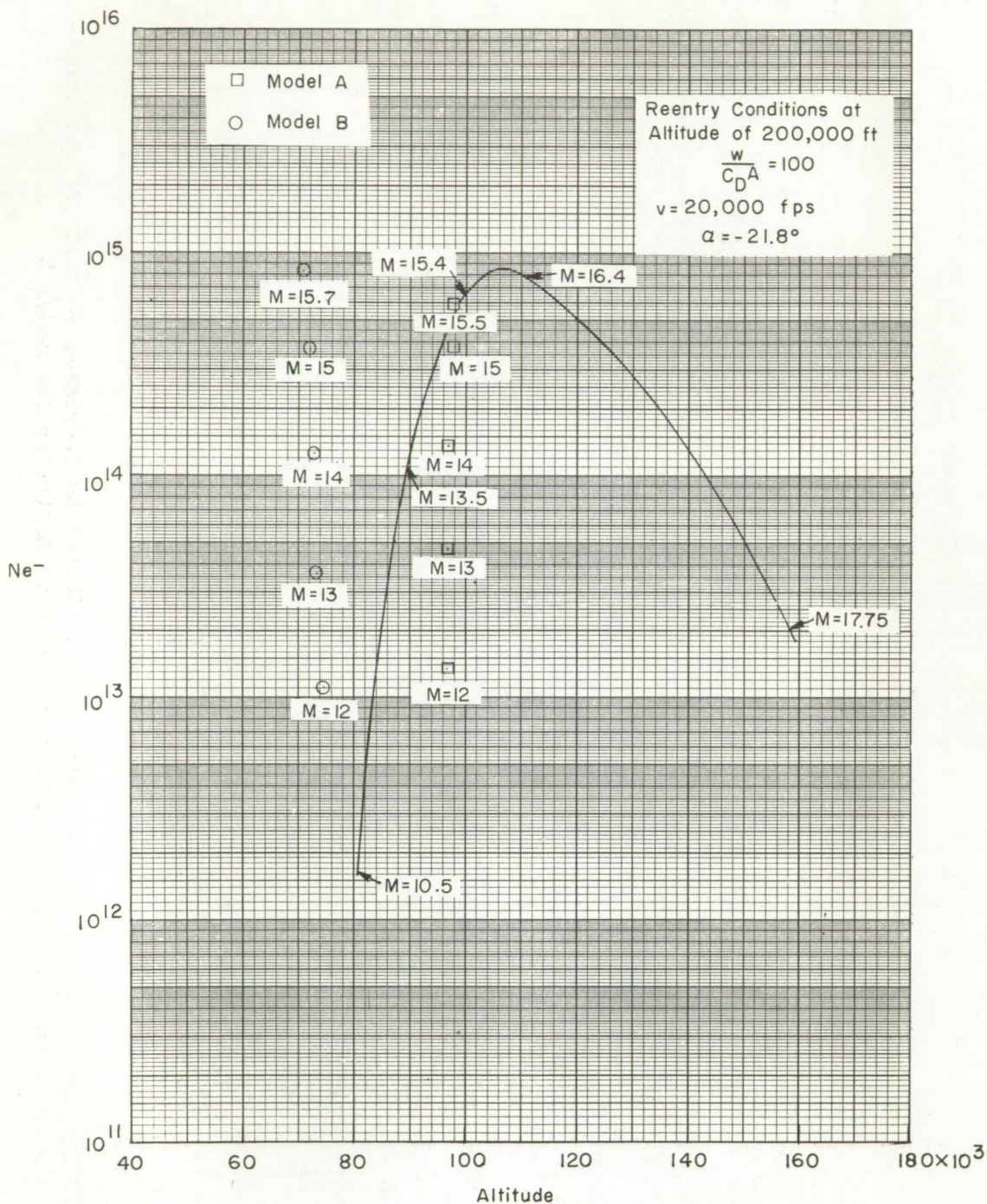
Figure 25.- Variation of electron concentration at stagnation point for hypothetical ballistic missile and models A and B.